NOAA OAR Special Report

PMEL Tsunami Forecast Series: Vol. x

A Tsunami Forecast Model for Westport, Washington

(Draft)

Liujuan Tang
Christopher D. Chamberlin

NOAA Center for Tsunami Research (NCTR)
Pacific Marine Environmental Laboratory

Contents

List of Tables

PMEL Tsunami Forecast Series: Vol. x
A Tsunami Forecast Model for Westport, WA

Liujuan Tang and Chris Chamberlin

Abstract

This study describes the development, validation, and testing of a tsunami forecast model for Westport, Washington. Based on the Method of Splitting Tsunamis (MOST) model, the forecast model is capable of simulating four hours of tsunami wave dynamics at a resolution of approximately 90 m in 10-minute computational time. A reference inundation model of higher resolution of 1/3 arc-sec (~10 m) was also developed in parallel, to provide modeling references for the forecast model. Both models were tested for fourteen past tsunamis and a set of eighteen simulated magnitude 9.3 tsunamis. The good agreement between the model computations and observations, along with the numerical consistency between the model results for the maximum amplitude and velocity, provide a quantitative validation and reliable robustness and stability testing of the forecast model.

1 Background and Objective

The National Oceanic and Atmospheric Administration (NOAA) Center for Tsunami Research at NOAA's Pacific Marine Environmental Laboratory (PMEL) has developed a tsunami forecasting system for operational use by NOAA's two Tsunami Warning Centers located in Hawaii and Alaska (Titov, 2005; Titov, 2009). The forecast system combines real-time deep-ocean tsunami measurements from Deep-ocean Assessment and Reporting of Tsunami (DART) buoys (*Gonzalez et al*., 2005; *Bernard et al.*, 2006, *Bernard and Titov*, 2007) with the Method of Splitting Tsunami (MOST) model, a suite of finite difference numerical codes based on nonlinear long wave approximation (*Titov and Synolakis*, 1998; *Titov and Gonzalez*, 1997; *Synolakis*, *et al*., 2008) to produce real-time forecasts of tsunami arrival time, heights, periods and inundation. To achieve accurate and detailed forecast of tsunami impact for specific sites, high-resolution tsunami forecast models are under development for United States coastal communities at risk (Tang *et al.*, 2008[a]; 2009[a]). The resolution of these models has to be high enough to resolve the dynamics of a tsunami inside a particular harbor, including influences of major harbor structures such as breakwaters. These models have been integrated as crucial components into the forecast system.

Presently, a system of 37 DART buoys (32 U.S.-, 1 Chilean-, and 4 Australian- owned) is monitoring tsunami activity in the Pacific Ocean (Figure 1) (48 DART buoys globally). The pre-computed propagation models currently have 1106 scenarios to cover Pacific tsunami sources (1691 globally), and the high-resolution forecast inundation models are now set up for 43 U.S. coastal communities. The fully implemented system will use real-time data from the DART

network to provide high-resolution tsunami forecasts for at least 75 communities in the U.S. (by 2013) (Titov, 2009). Since its first testing in the 17 November 2003 Rat Island tsunami, the forecast system has produced experimental real-time forecasts for twelve tsunamis in the Pacific and Indian oceans (*Titov et al.*, 2005; *Wei et al*., 2008; *Titov*, 2009). The forecast methodology has also been tested with the data from nine additional events that produced the deep ocean data.

The report describes the development, testing and applications of the Kahului forecast model. The objective in developing this model is to provide NOAA's Tsunami Warning Centers the ability to assess danger posed to Kahului following tsunami generation in the Pacific Ocean Basin with a goal to provide accurate and timely forecasts to enable the community to respond appropriately. A secondary objective is to explore the potential tsunami impact from earthquakes at major subduction zones in Pacific to the city by using the developed forecast model. Wavelet analysis was applied to investigate Kahului harbor and local responses to tsunami waves.

The report is organized as follows. Section 2 briefly introduces NOAA's tsunami forecast methodology. Section 3 describes the model development. Section 4 presents the results and discussion, which includes sensitivity of the forecast model to model setup and friction coefficients, model validation, verification, and testing for past and simulated tsunamis. A tsunami hazard assessment study utilizing the validated forecast model is also included. A summary and conclusion are provided in section 5.

2 Forecast Methodology

NOAA's real-time tsunami forecasting scheme is a process that comprises of two steps: (1) construction of a tsunami source via inversion of deep ocean DART observations with pre-computed tsunami source functions; and (2) coastal predictions by running high-resolution forecast models in real time (*Titov et al*., 1999; *Titov et al*., 2005; Tang *et al*., 2009[a]). The DART-constrained tsunami source, the corresponding offshore scenario from the tsunami source function database, and high-resolution forecast models cover the entire evolution of earthquake-generated tsunamis, generation, propagation and coastal inundation, providing a complete tsunami forecast capability.

2.1 Construction of A Tsunami Source Based on DART Observations and Tsunami Source Functions

Several real-time data sources, including seismic data, coastal tide gage and deep-ocean data have been used for tsunami warning and forecast (*Satake et al*., 2008; *Whitmore*, 2003; *Titov,* 2009). NOAA's strategy for the real-time forecasting is to use deep-ocean measurements at DART buoys as the primary data source due to several key features. (1) The buoys provide a direct measure of tsunami waves, unlike seismic data, which are an indirect measure of tsunamis. (2) The deep ocean tsunami measurements are in general the earliest tsunami information available, since tsunamis propagate much faster in deep ocean than in shallow coastal area where coastal tide gages are used for tsunami measurements. (3) Compared to coastal tide gages, DART data with a high signal to noise ratio can be obtained without interference from harbor

and local shelf effects. (4) Wave dynamics of tsunami propagation in deep ocean is assumed to be linear (Liu, 2009). This linear process allows application of efficient inversion schemes.

Time series of tsunami observations in deep-ocean can be decomposed into a linear combination of a set of tsunami source functions in the time domain by a linear least squares method. We call coefficients obtained through this inversion process *tsunami source coefficients*. The magnitude computed from the sum of the moment of tsunami source functions multiplied by the corresponding coefficients is referred as the *tsunami moment magnitude* (T_{Mw}), to distinguish from the seismic moment magnitude M_w, which is the magnitude of the associated earthquake source. While the seismic and tsunami sources are in general not the same, this approach provides a link between the seismically-derived earthquake magnitude and the tsunami observation-derived tsunami magnitude.

During real-time tsunami forecast, seismic waves propagate much faster than tsunami waves so the initial seismic magnitude can be estimated before the DART measurements are available. Since time is of the essence, the initial tsunami forecast is based on the seismic magnitude only. The T_{Mw} will update the forecast when it is available via DART inversion using the tsunami source function database.

Titov et al.(1999; 2001) conducted sensitivity studies on far-field deep-water tsunamis to different parameters of elastic deformation model described in *Gusiakov* (1978) and *Okada* (1985). The results showed source magnitude and location essentially define far-field tsunami signals for a wide range of subduction zone earthquakes. Other parameters have secondary influence and can be pre-defined during forecast. Based on these results, tsunami source function databases for Pacific, Atlantic, and Indian Oceans have been built using pre-defined source parameters, length = 100 km, width = 50 km, slip = 1 m, rake = 90 and rigidity = 4.5 x 10^{10} N/m^2. Other parameters are location-specific; details of the databases are described in *Gica et al*. (2008). Each tsunami source function is equivalent to a tsunami from a typical M_w = 7.5 earthquake with defined source parameters. Figure 1 shows the locations of tsunami source functions in Pacific Ocean.

The database can provide offshore forecast of tsunami amplitudes and all other wave parameters immediately once the inversion is complete. The tsunami source, which combines real-time tsunami measurements with tsunami source functions, provides an accurate offshore tsunami scenario without additional time-consuming model runs.

2.2 Real-time Coastal Predictions by High-Resolution Forecast Models.

High-resolution forecast models are designed for the final stage of the evolution of tsunami waves: coastal runup and inundation. Once the DART-constrained tsunami source is obtained (as a linear combination of tsunami source functions), the pre-computed time series of offshore wave height and depth-averaged velocity from the model propagation scenario are applied as the dynamic boundary conditions for the forecast models. This saves the simulation time of basin wide tsunami propagation. Tsunami inundation is a highly nonlinear process, therefore a linear combination would not, in general, provide accurate solutions. A high-resolution model is also required to resolve shorter tsunami wavelengths nearshore with accurate bathymetric/topographic data. The forecast models are constructed with the Method of Splitting

Tsunami (MOST) model, a finite difference tsunami inundation model based on nonlinear shallow-water wave equations (*Titov and Gonzalez,* 1997). Each forecast model contains three telescoping computational grids with increasing resolution, covering regional, intermediate and nearshore areas. Runup and inundation are computed at the coastline.

The highest resolution grid includes the population center and tide stations for forecast verification. The grids are derived from the best available bathymetric/topographic data at the time of development, and will be updated as new survey data become available.

The forecast models are optimized for speed and accuracy. By reducing the computational areas and grid resolutions, each model is optimized to provide 4-hour event forecasting results in minutes of computational time using one single processor, while still providing good accuracy for forecasting. To ensure forecast accuracy at every step of the process, the model outputs are validated with historical tsunami records and compared to numerical results from a reference inundation model with higher resolutions and larger computational domains. In order to provide warning guidance for long duration during a tsunami event, each forecast model has been tested to output up to 24-hour simulation since tsunami generation.

3 Model Development

3.1 Forecast area and tsunami data

Grays Harbor is an estuarine bay located on the southwest Pacific coast of Washington state (Fig. 2a). The bay is 17 miles (27 km) long and 12 miles (19 km) wide. The Chehalis River flows into its eastern end, where the city of Aberdeen stands at that river's mouth, on its north bank, with the somewhat smaller city of Hoquiam immediately to its northwest, along the bayshore. The northern peninsula is largely covered by the community of Ocean Shores, while the southern peninsula stands the town of Westport.

Westport Marina is the largest coastal marina in the Pacific Northwest and home to Washington State's largest charter fishing fleet (Fig.2b). This full-service Marina offers moorage space for 600 charter, commercial, and sport fishing vessels, plus a wide range of pleasure craft. A Nation Ocean Service water level station in Westport Marina was established on June 7th, 1982. The present installation was on March 20th, 2006 (http://tidesandcurrents.noaa.gov/). The water level sensor is located in the vicinity of the Chevron fuel pier in Westport Marina. At the sensor, the mean tidal range (MN) is 2.119 m, mean sea level (MSL) is 2.386 m, and mean high water level (MHW) is 3.451 m, and. Mean high water is used as the reference level for the forecast model to provide a worst case for inundation forecast.

Figure 3 shows the population density data in the Grays Harbor County. The population in Aberdeen ranks the highest, 16,440 as in 2009, while 8,765 in Hoquiam, 4,860 in Ocean Shores, and 2,345 in Westport (http://www.ghedc.com/tblcensus.html#population).

Tsunami time series data are available for four past tsunamis since 2006 at the Westport tide station. The largest wave height of 25 cm was recorded during the 15 November 2006 Kuril Islands tsunami.

3.2 Bathymetry and Topography

Two digital elevation models (DEMs) were developed, One with medium resolution of 3 arc-second (90 m), which was developed at NCTR in 2010, covering the Pacific coast in Washington; and a high resolution DEM of 1/3 arc-second (10 m) covering Westport, WA and Astoria, Oregon (Fig. 6) developed at NGDC (Tylor et al., 2008). Both grids include topographic and bathymetric elevations. The source grids were compiled from the best available data sources at the time of development.

3.3 Model Setup

By sub-sampling from the DEMs described in section 3.2, two sets of computational grids were derived, the Westport reference inundation model (Fig. 4) and the optimized forecast model (Fig. 5). The forecast model consists of three levels of telescoped grids with increasing resolution, while the reference model has four grids to better resolve the fine structure of the Westport Marina. In Figure 4, the solid boxes in red indicate boundaries of the nested reference model grids while the black dashed boxes represent the corresponding boundaries of the forecast model. Grid details at each level and input parameters are summarized in Table 2. For a simulation of a 4-hour event, the optimized forecast model takes less than 10 minutes of CPU time on a Linux system using a single 3.6 GHz Xeon processor, while the reference model takes about 41 hours.

4 Results and discussion

4.1 Validation

Both the Westport reference and forecast models were tested with sixteen historical tsunamis summarized in Table 1. Figure 6 shows the modeling results and observations at the Westport tide station. The observations from the 2007 Kuril Islands tsunami are within the noise level (Fig. 5.2). Tsunami time series data are available for four past tsunamis, the 2006 Tonga, 2006 Kuril Islands, 2009 Samoa and 2010 Chile tsunamis at the Westport tide station. The modeled amplitudes agree reasonable with the observations. Most of the data are with low signal to noise ratio and unable to indentify the arrival time of the tsunamis. The largest wave height of 25 cm was recorded during the 15 November 2006 Kuril Islands tsunami.

4.2 Verification

The computed maximum water elevation above MHW and maximum velocity of the sixteen tsunamis are plotted in Figure 7. Both the reference and forecast models produced similar patterns and values. The open coast experiences high amplitude waves than those within the Grays Harbor.

4.3 Robustness and stability tests

Recorded historical tsunamis provide only a limited number of events, from limited locations. More comprehensive test cases of destructive tsunamis with different directionalities are needed to check the stability and robustness for the forecast model. The same set of eighteen simulated T_{Mw} 9.3 tsunamis as in Tang *et al*. (2008[a], 2009[b]) was selected here for further examination. Results computed by the forecast model are compared with those from the high-resolution reference model in Figures 8 and 9. Both models were numerically stable for all of the scenarios. In general, waveforms and maximum water elevation computed by the forecast model agree well with those from the reference model in most of the forecast area. One exception is with inside the Marina when the first waves exceed 2 m. For example, the forecast model overestimate the first peak (4.5 m) for the Mw 9.3 Cascadia scenario while the reference model shows 2.5m. That is due to the 3-sec resolution for the forecast model is unable to well resolve the small entrances and breakwater for Westport Marina. A D-grid just cover the Marina with finer resolution can be implemented in the forecast model with the MOST version 4 in the future.

Tsunami waves in the study area vary significantly for the eighteen magnitude 9.3 scenarios. These results show the complexity and high nonlinearity of tsunami waves nearshore, which again demonstrate the value of the forecast model for providing accurate site-specific forecast details. The No. 5 and 6 scenarios at Cascadia subduction generate severe inundation in the open coast. The computed maximum water elevation reaches nearly 4.5 m at the tide station.

5 Summary and Conclusions

A tsunami forecast model was developed for the coastal community of Westport, Washington. The computational grids for the forecast model were derived from the best available bathymetric and topographic data sources. The forecast model is optimizedly constructed at a resolution of 3-arc-sec (~90 m) to enable a 4-hr inundation simulation within 10-minute computational time. A reference inundation model of higher resolution of 1/3 arc-sec (~10 m) was also developed in parallel, to provide modeling references for the forecast model. Both models were tested for fourteen past tsunamis and a set of eighteen simulated magnitude 9.3 tsunamis.

The modeled amplitudes agree reasonable with the observations at Westport tide station for four past tsunamis. The open coast experiences high amplitude waves than those within the Grays Harbor or Westport Marina.

Both models were numerically stable for all of the tested scenarios. In general, waveforms and maximum water elevation computed by the forecast model agree well with those from the reference model in most of the forecast area except within the Westport Marina the forecast model overestimate the first peak when it is exceed 2 m. That is due to the 3-sec resolution for the forecast model is unable to well resolve the small entrances and breakwater for Westport Marina. A D-grid just cover the Marina with finer resolution can be implemented in the forecast model with the MOST version 4 in the future.

Tsunami waves in the study area vary significantly for the eighteen magnitude 9.3 scenarios. These results show the complexity and high nonlinearity of tsunami waves nearshore, which again demonstrate the value of the forecast model for providing accurate site-specific forecast details. The No. 5 and 6 scenarios at Cascadia subduction generate severe inundation in the open coast. The computed maximum water elevation reaches nearly 4.5 m at the tide station.

The study suggests considering points on the open coast as warning points for this area beside the Westport tide gage, due to its protection from the open coast by both the Grays Harbor and the Westport Marina with narrow entrance and breakwaters.

Acknowledgements

The author thank Jean Newman for assistance with the propagation database; Marie Eble, Nazila Merati and Lindsey Waller for assistance with La Push tide gage data; Chris Chamberlin and Kelly Carignan for help with DEMs; Chris Moore for MOST versioning; and Ryan L. Whitney for comments and editing.

This research is funded by the NOAA Center for Tsunami Research (NCTR) xxxx. This publication is partially funded by the Joint Institude for the Study of the Atmosphere and Ocean (JISAO) under NOAA Cooperative Agreement No. NAxxxxx, Contribution #xxxx.

References

Allen, A.L., N.A. Donoho, S.A. Duncan, S.K. Gill, C.R. McGrath, R. S. Meyer, M. R. Samant (2008), NOAA's National Ocean Service Supports Tsunami Detection and Warning through Operation of Coastal Tide Stations, In: Solutions to Coastal Disasters 2008 /Tsunamis/: Proceedings of Sessions of the Conference, April 13-16, 2008 Turtle Bay, Oahu, Hawaii. American Society of Civil Engineers.

Berkman, S.C. and J.M. Symons (1964), The tsunami of May 22, 1960 as recroded at tide stations, U.S. Dept. of Commerce, C&GS, Washington 25, D.C., 69 pp.

Bernard, E.N., H.O. Mofjeld, V.V. Titov, C.E. Synolakis, and F.I. González (2006): Tsunami: Scientific frontiers, mitigation, forecasting, and policy implications. Proc. Roy. Soc. Lon. A, 364(1845), doi: 10.1098/rsta.2006.1809, 1989–2007.

Bernard, E., and V.V. Titov (2007), Improving tsunami forecast skill using deep ocean observations, Mar. Technol. Soc. J., 40(3), 23–26.

Fraser, G.D., P.J. Eaton and C.K. Wentworth (1959) The tsunami of March 9, 1957, on the Island of Hawaii, *Bulletin of the Seismological Society of America*; January 1959; v. 49; no. 1; p. 79-90

Green, C.K. (1946): Seismic sea wave of April 1, 1946, as recorded on tide gages. *Transactions, American Geophysical Union*, 27, 490-500.

Gica E., Spillane, M.C., Titov, V.V., Chamberlin, C.D. and Newman, J.C. (2008), Development of the forecast propagation database for NOAA's Short-Term Inundation Forecast for Tsunamis (SIFT), NOAA Tech. Memo. OAR PMEL-139, 89pp.

Gusiakov, V.K. (1978): Static displacement on the surface of an elastic space. Ill-posed problems of mathematical physics and interpretation of geophysical data, Novosibirsk, VC SOAN SSSR, 23–51 (in Russian).

Gonzalez, F.I., E.N. Bernard, C. Meinig, M. Eble, H.O. Mofjeld, and S. Stalin (2005): The NTHMP tsunameter network. *Nat. Hazards*, 35(1), Special Issue, U.S. National Tsunami Hazard Mitigation Program, 25-39.

Little, M. (2006): Personal e-mail communication to NOAA, National Ocean Service Center for Operational Oceanographic, Products and Services.

Liu, P. L.-F. (2009), Tsunami modeling—Propagation, in The Sea, vol. 15, edited by E. Bernard and A. Robinson, chap. 9, pp. 295– 319, Harvard Univ. Press, Cambridge, Mass.

López, A.M. and E.A. Okal (2006): A seismological reassessment of the source of the 1946 Aleutian 'tsunami' earthquake, *Geophysical Journal International*, Volume 165, Issue 3, Page 835-849, Jun 2006, doi: 10.1111/j.1365-246X.2006.02899.x

Johnson, J.M., Y. Tanioka, L.J. Ruff, K. Satake, H. Kanamori and L.R. Sykes (1994): The 1957 Great Aleutian Earthquake. *Pure and Applied Geophysics*, 142(1), 3-28.

Johnson, J.M., K. Satake, S.R. Holdahl and J. Sauber (1996): The 1964 Prince William earthqake: Joint inversion of tsunami and geodetic data. *Journal of Geophysical Research*, 101(B1), 523-532.

Johnson, J.M. and K. Satake (1999): Asperity distribution of the 1952 Great Kamchatka earthquake and its relation to future earthquake potential in Kamchatka. *Pure and Applied Geophysics*, 154(3-4), 541-553.

Kanamori, H. and J.J. Ciper (1974): Focal process of the great Chilean earthquake, May 22, 1960. *Physics of the Earth and Planetary Interiors*, 9, 128-136.

Maui County (2006): The Maui Shoreline Atlas.
http://www.co.maui.hi.us/departments/Planning/erosion.htm

National Geophysical Data Center, Global Tsunami Database (2000 BC to present):
http://www.ngdc.noaa.gov/seg/hazard/tsu_db.shtml

NOAA/NOS (1991): Next Generation Water Level Measurement System (NGWLMS) Site Design, Preparation, and Installation Manual, NOAA/NOS, January 1991.

Okada, Y., 1985, Surface deformation due to shear and tensile faults in a half-space. *Bull. Seismol. Soc. Am*., 75, 1135-1154.

Salsman, G. G. (1959): The tsunami of March 9, 1957, as recorded at tide stations. U.S. Coast and Geodetic Survey, 18 pp.

Satake, K., Y. Hasegawa, Y. Nishimae and Y. Igarashi (2008), Recent Tsunamis That Affected the Japanese Coasts and Evaluation of JMA's Tsunami Warnings. OS42B-03, AGU Fall Meeting, San Francisco.

Shepard, F.P., G.A. Macdonald and D.C. Cox (1950): Tsunami of April 1, 1946, *Bulletin Scripps Institution of Oceanography*, 5: 391-528.

Smith, W. H. F., and D. T. Sandwell (1997), Global seafloor topography from satellite altimetry and ship depth soundings, Science, 277, 1957– 1962.

Spaeth, M.G. and S.C. Berkman (1967): The Tsunami of March 28, 1964, as Recorded at Tide Stations. Coast and Geodetic Survey Technical Bulletin No. 33, Rockville, Md, 86 pp.

Soloviev, S.L., Ch.N Go and Kh.S Kim (1992): *Catalog of Tsunamis in The Pacific* 1969-1982. Results of Researches on The International Geophysical Projects, Academy of Sciences of the USSR Soviet Geophysical Committee, Moscow, 1992, 208 pp.

Synolakis, C.E., E.N. Bernard, V.V. Titov, U. Kânoğlu, and F.I. González (2008): Validation and verification of tsunami numerical models. *Pure Appl. Geophys*., 165(11–12), 2197–2228.

Tang, L., C. Chamberlin, E. Tolkova, M. Spillane, V.V. Titov, E. N. Bernard and H. O. Mofjeld (2006): Assessment of Potential Tsunami Impact for Pearl Habor, Hawaii. NOAA Technical Memorandum OAR PMEL-131, August 2006, 36 pp.

Tang, L., C. Chamberlin and V.V. Titov, (2008a), Developing tsunami forecast inundation models for Hawaii: procedures and testing, *NOAA Tech. Memo., OAR PMEL -141*, 46 pp.

Tang, L., V. V. Titov, Y. Wei, H. O. Mofjeld, M. Spillane, D. Arcas, E. N. Bernard, C. Chamberlin, E. Gica, and J. Newman (2008b), Tsunami forecast analysis for the May 2006 Tonga tsunami, J. Geophys. Res., 113, C12015, doi:10.1029/2008JC004922.

Tang, L., V. V. Titov, and C. D. Chamberlin (2009a), Development, Testing, and Applications of Site-specific Tsunami Inundation Models for Real-time Forecasting, *J. Geophys. Res*., doi:10.1029/2009JC005476, in press.

Tang, L., V.V. Titov and C.D. Chamberlin (2009b), A Tsunami Forecast Model for Hilo, Hawaii, NOAA OAR Special Report, PMEL Tsunami Forecast Series: Vol. 1, 44 pp.

Taylor, L.A., B.W. Eakins, K.S. Carignan, and R.R. Warnken (2008) Digital Elevation Model for Astoria, Oregon: Procedures, Data Sources and Analysis, May 30, 2008.

Titov, V.V. (2009), Tsunami forecasting. Chapter 12 in *The Sea*, Volume 15: Tsunamis, Harvard University Press, Cambridge, MA and London, England, 371–400.

Titov, V.V., F.I. González, E.N. Bernard, M.C. Eble, H.O. Mofjeld, J.C. Newman, and A.J. Venturato (2005): Real-time tsunami forecasting: Challenges and solutions. *Natural Hazards*, 35(1), Special Issue, U.S. National Tsunami Hazard Mitigation Program, 41–58.

Titov, V. V., Mofjeld, H. O., Gonza´ lez, F. I., and Newman, J. C.: 2001, Offshore forecasting of Alaskan tsunamis in Hawaii. In: G. T. Hebenstreit (ed.), Tsunami Research at the End of a Critical Decade. Birmingham, England, Kluwer Acad. Pub., Netherlands, pp. 75–90.

Titov, V.V., H.O. Mofjeld, F.I. Gonzalez and J.C. Newman (1999): Offshore forecasting of Alaska-Aleutian subduction zone tsunamis in Hawaii. NOAA Technical Memorandum. ERL PMEL-114, January 1999, 22 pp.

Titov, V.V. and C.S. Synolakis (1998): Numerical modeling of tidal wave runup. *Journal of Waterway, Port, Coastal and Ocean Engineering*, ASCE, 124(4), 157-171.

Titov, V.V. and F.I. Gonzalez (1997): Implementation and testing of the Method of Splitting Tsunami (MOST) model. NOAA Technical Memorandum. NOAA Pacific Marine Environmental Laboratory, ERL PMEL-112, Nov. 1997, 11 pp.

Pararas-Carayannis, G.(1969): *Catalog of Tsunamis in The Hawaii Islands*, World Data Center A Tsunami, ESSA – Coast and Geodetic Survey, 94 pp.

USGS (2007), M 8.1 Kuril Islands Earthquake of 13 January 2007, Earthquake Summary Map XXX, U.S Geological Survey.

Walker, D.A. (2004): Regional Tsunami evacuations for the state of Hawaii: a feasibility study on historical runup data. Science of Tsunami Hazards, 22(1), 3-22.

Wei, Y., E. Bernard, L. Tang, R. Weiss, V. Titov, C. Moore, M. Spillane, M. Hopkins, and U. Kânoğlu (2008): Real-time experimental forecast of the Peruvian tsunami of August 2007 for U.S. coastlines. *Geophys. Res. Lett*., 35, L04609, doi: 10.1029/2007GL032250.

Whitmore, P.M. (2003), Tsunami amplitude prediction during events: A test based on previous tsunamis. In *Science of Tsunami Hazards*, 21, 135–143.

Zerbe, W.B. (1953), The tsunami of November 4, 1953 as recorded at tide stations. Special publication No. 300, Coast and Geodetic Survey, U.S. Department of Commerce, Government Printing Office, Washington 25 D.C., 62 pp.

Tables and Figures

Table 1 Tsunami sources and maximum wave height recorded at Kahului tide station for fourteen past tsunamis.

No.	Tsunami ID	Area	Earthquake Date Time (UTC)	Location Lat (°)	Location Lon (°)	Sub. zone	Seismic magnitude (M_W)	Tsunami magnitude	Tsunami source
1	194604	Unimak	1946.04.01 12:28:56	53.32N	163.19W	AACC	8.5 (Lopez&Okal, 2006)	[2]8.5	7.5*b23+19.7*b24+3.7*b25
2	195211	Kamchatka	1952.11.04 16:58:26.0	52.75N	159.50E	KKJI	9.0 (USGS)	[2]8.7	
3	195703	Andreanof	1957.03.09 14:22:31.9	51.292N	175.629W	AACC	8.6 (USGS)	[2]8.7	31.4*a15+10.6*a16+12.2*a17
4	196005	Chile	1960.05.22 19:11:14	39.5S	74.5W	SASZ	9.5 (Kanamori & Cipar, 1974)		
5	196403	Alaska	1964.03.28 03:36:14	61.10N	147.50W	AACC	9.2 (USGS)	[2]9.0	Tang *et al*. (2006)
6	199410	West Kuril Is.	1994.10.04 13:23:28.5	43.6N	147.63E	KKJI	8.3 (CMT)	8.1	9.00*a20
7	199606	Andreanof	1996.06.10 04:04:03.4	51.478N	177.41W	AACC	7.9 (CMT)	7.8	2.40*a15+0.80*b16
8	200106	Peru	2001.06.23 20:34:23.3	17.28S	72.71W	SASZ	8.4 (CMT)	8.2	5.70*a15+2.90*b16+1.98*a16
9	200309	Hokkaido	2003.09.25 19:50:38.2	42.21N	143.84E	KKJI	8.3 (CMT)	8.0	3.6m*(100x100km), 109#rake, 20#dip, 230#strike, 25m depth
10	200311	Rat Is.	2003.11.17 06:43:31	51.14N	177.86E	AACC	7.7 (CMT)	7.8	[1]2.81*b11
11	200605	Tonga	2006.05.03 15:26:39	20.39S	173.47W	NZKT	8.0 (CMT)	8.0	6.6*b29 (Tang *et al*., 2008[1])
12	200611	Kuril Is.	2006.11.15 11:15:8.0	46.71N	154.33E	KKJI	8.3 (CMT)	8.1	[1]4*a12+0.5*b12+2*a13+1.5*b13
13	200701	Kuril Is.	2007.01.13 04:23:48.1	46.17N	154.80E	KKJI	8.1 (CMT)	7.9	-3.64*b13
14	200708	Peru	2007.08.15 23:41:57.9	13.73S	77.04W	SASZ	8.0 (CMT)	8.1	[1]4.1*a9+4.32*b9 (Wei *et al*., 208)
15	200929	Samoa	2009.09.29 17:48:26.8	15.13S	171.97W	NTSZ	8.1	8.1	3.96xa34+3.96xb34
16	201002	Chile	2010.02.27 6:35:15.4	35.95S	73.15W	CSSZ	8.8	8.8	

1: The tsunami source was obtained during real time and applied to forecast.
2: Preliminary result.
3. Trough reached gage limit.

Table 2 MOST setups of Westport reference and forecast models.

Grid	Region	Reference Model			Forecast model		
		Coverage Lon. (^{0}E) Lat. (^{0}N)	Cell Size (")	Time Step (sec)	Coverage Lon. (^{0}E) Lat. (^{0}N)	Cell Size (")	Time Step (sec)
A	WA	226.0-237.0 43.00 – 52.00	36 (1101 x 901)	3.0	232.945-236.945 44.6833-48.95	120 (121 x 129)	14
B	Southwest WA	234.95 – 236.9 45.96 – 47.30	6 (1171 x 805)	0.6	234.95 - 236.40 46.335 – 47.30	18 (291 x 194)	2
C	Grays Harbor	235.75 – 236.25 46.8333 – 47.0833	4/3 x 1 (1351 x 901)	1.2	235.75 - 236.25 46.8333-47.0833	5 x3 (361x301)	2
D	Westport	235.7541– 235.9519 46.8643 – 46.9621	1/3 (2137 x 1057)	0.3			
Minimum offshore depth (m)		1			1		
Water depth for dry land (m)		0.1			0.4		
Friction coefficient (n^2)		0.0009			0.0009		
Computational time for a 4-hr simulation		~ 41 hours			**< 10 minutes**		

Appendix A.

Since the initial development of the forecast model for Westport, Washington, the parameters for the input file for running the forecast and reference models have been changed to reflect changes to the MOST model code. The following appendix lists the new input files for Westport.

A1. Reference model *.in file for Westport, Washington—updated for 2010

```
0.001       Minimum amplitude of input offshore wave (m):
1           Input minimum depth for offshore (m)
0.1         Input "dry land" depth for inundation (m)
0.0009      Input friction coefficient (n**2)
1           runup flag for grids A and B (1=yes,0=no)
300.0       blowup limit
0.3         Input time step (sec)
72000       Input amount of steps
10          Compute "A" arrays every n-th time step, n=
2           Compute "B" arrays every n-th time step, n=
4           Compute "C" arrays every n-th time step, n=
```

150	Input number of steps between snapshots
1	...Starting from
1	...Saving grid every n-th node, n=

A2. Forecast model *.in file for Westport, Washington—updated for 2010

0.0001	Minimum amplitude of input offshore wave (m):
1	Input minimum depth for offshore (m)
0.4	Input "dry land" depth for inundation (m)
0.0009	Input friction coefficient (n**2)
1	runup flag for grids A and B (1 = yes, 0 = no)
300.0	blowup limit
2.0	Input time step (sec)
9600	Input amount of steps
7	Compute "A" arrays every n-th time step, n=
1	Compute "B" arrays every n-th time step, n=
14	Input number of steps between snapshots
1	…Starting from
1	…Saving grid every n-th node, n=

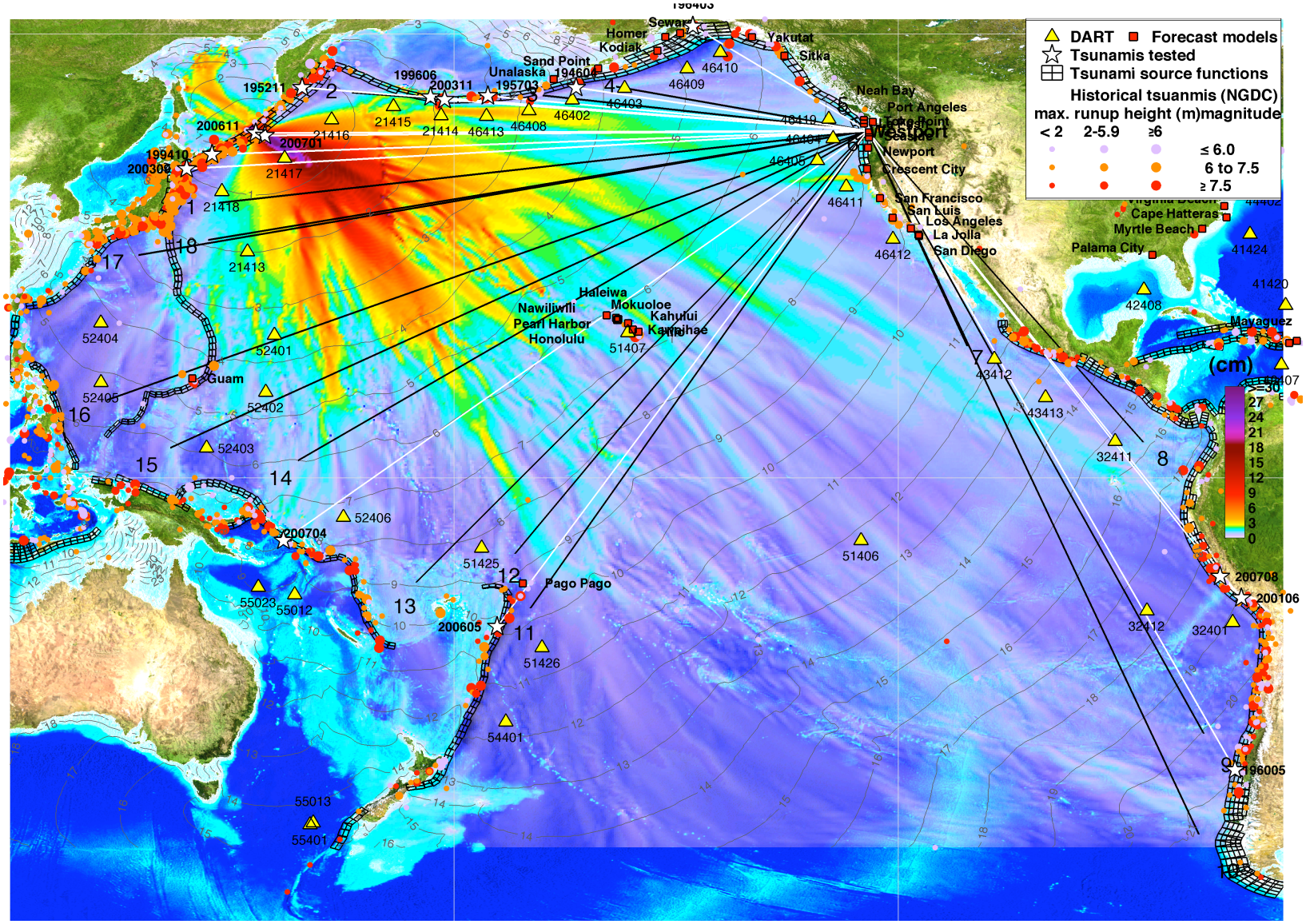

Figure 1 Overview of the Tsunami Forecast System. Filled colors show the offshore forecast of the maximum computed tsunami amplitude in cm for the 13 January 2007 Kurile Islands tsunami in the Pacific. Contours indicate the first arrival time in hours. White lines, sixteen past tsunamis and black lines, eighteen simulated tsunamis tested in this study.

Figure 2 Aerial photos of (a) Gray's Harbor and (b) Westport Marina.

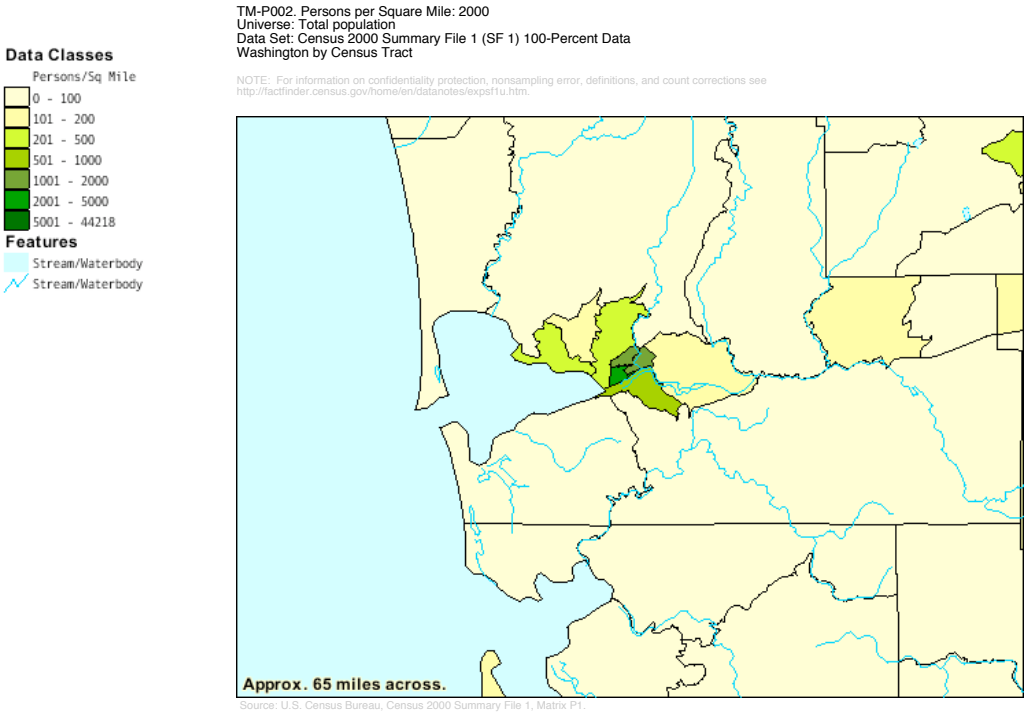

Figure 3 Population density (2000 Census) .

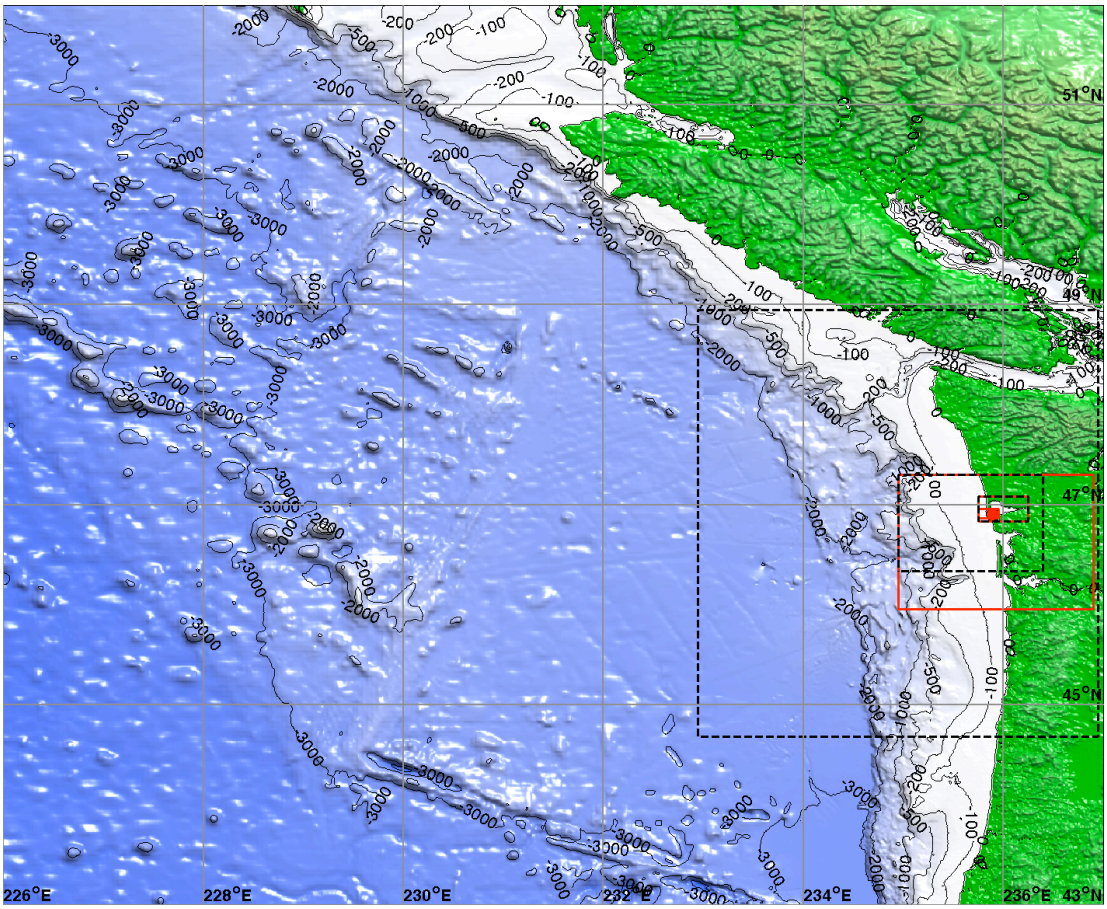
51°N
49°N
47°N
45°N
43°N
226°E
228°E
230°E
232°E
234°E
236°E

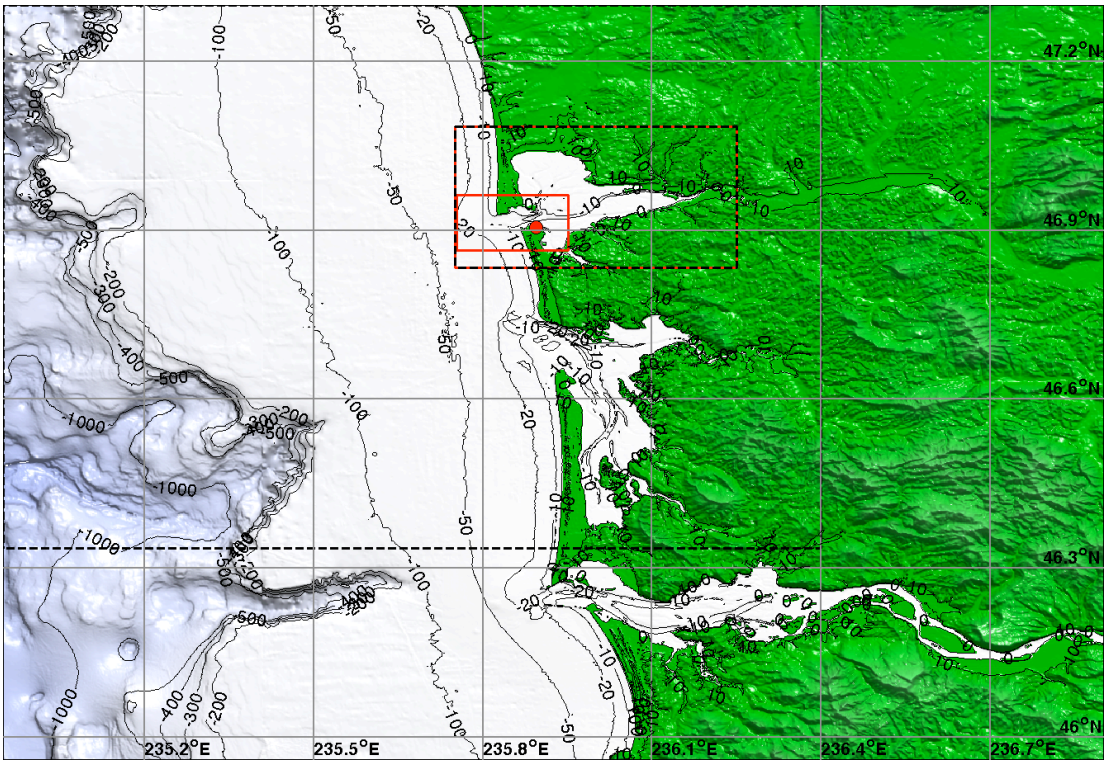
47.2°N
46.9°N
46.6°N
46.3°N
46°N
235.2°E
235.5°E
235.8°E
236.1°E
236.4°E
236.7°E

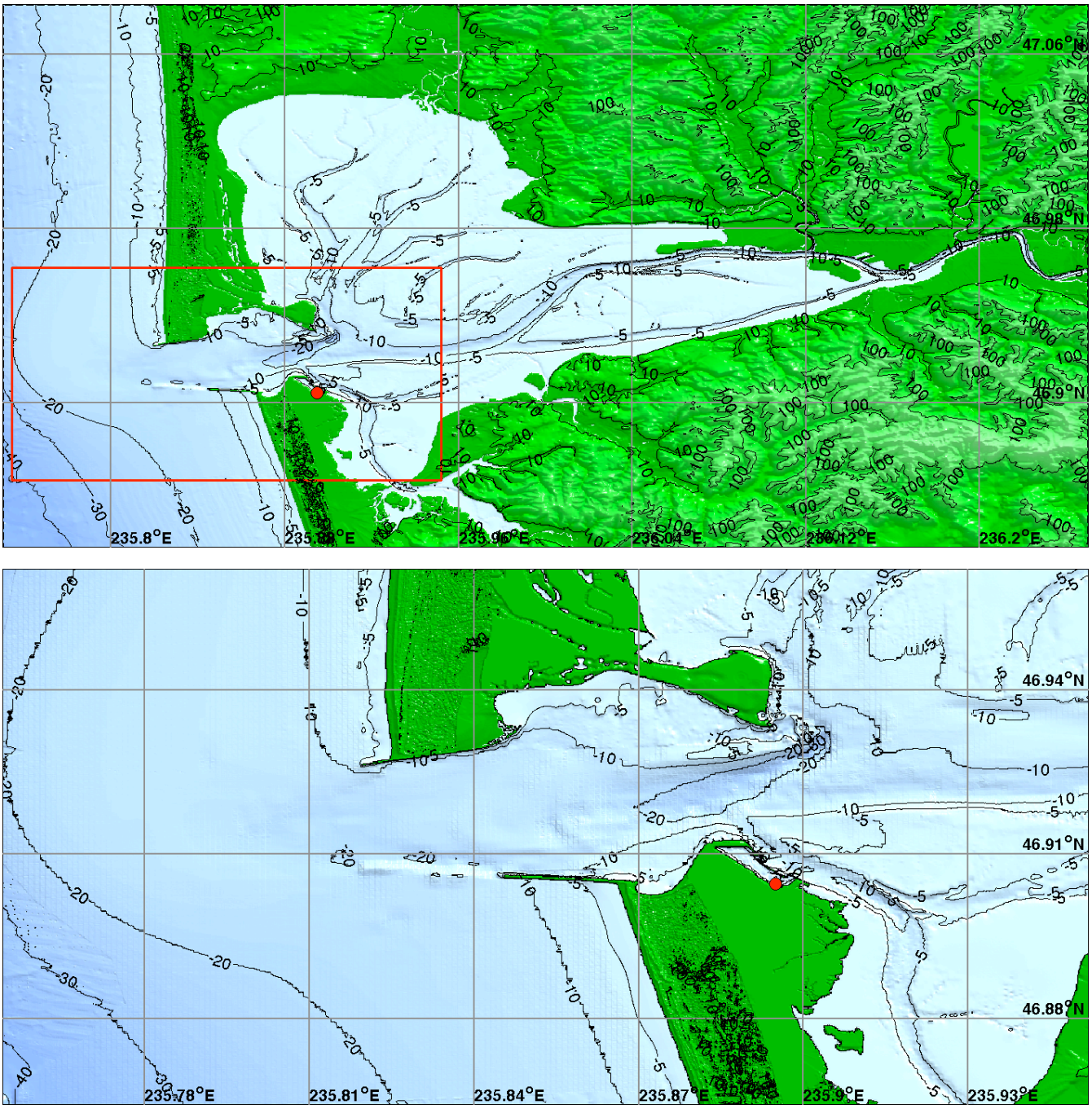

Figure 4 Four layers of grid setup for Westport reference model with resolutions of (2) 36 arc-sec, (b) 6 arc-sec, (c) 1 sec (~30 m) and (d) 1/3 arc-sec (~10 m). Red boxes, boundaries of the telescoping grids for the reference model; black dashed boxes, grid boundaries of the forecast model.

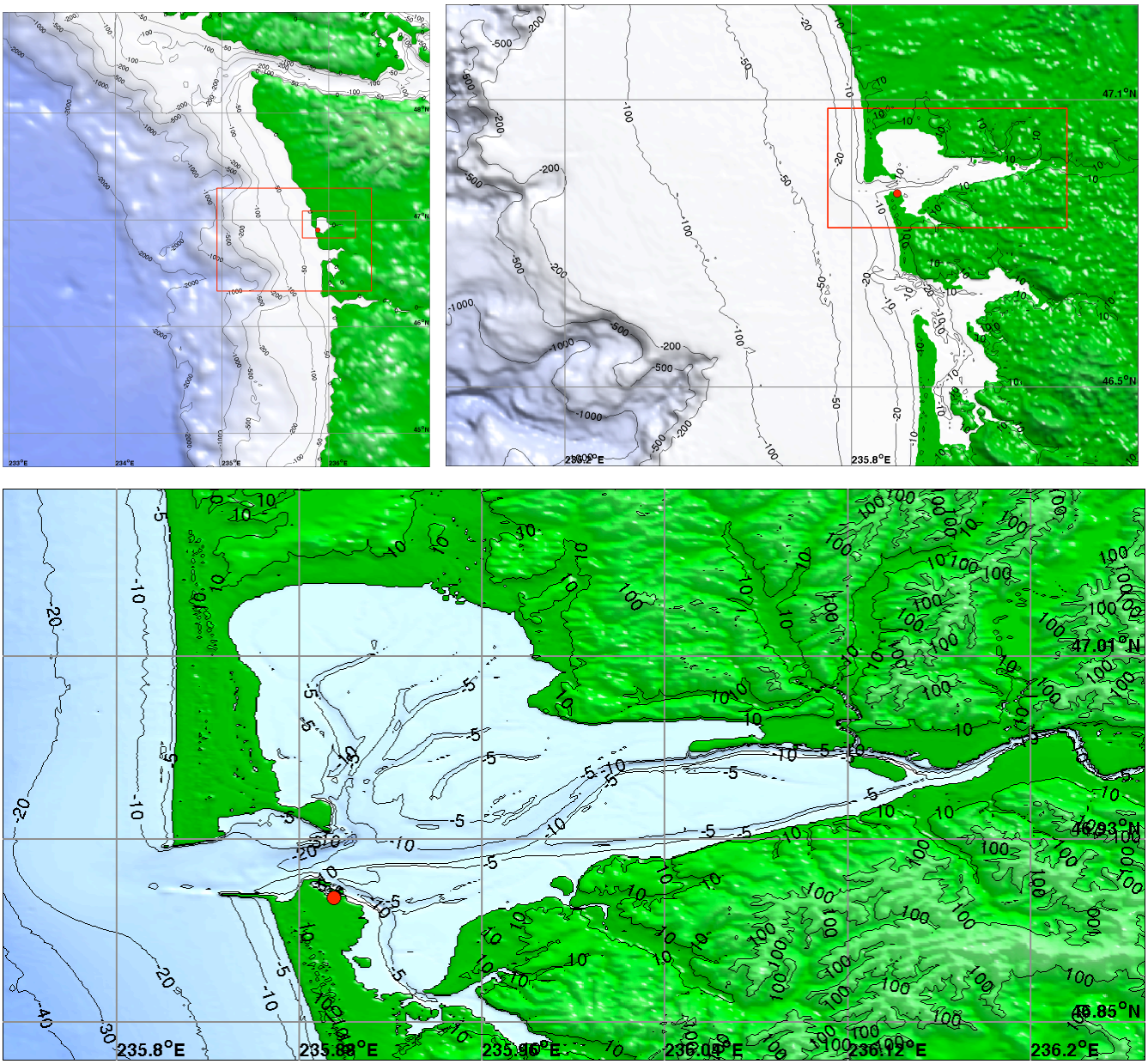

Figure 5 Three layers of grid setup for Westport forecast model with resolutions of (2) 120 arc-sec, (b) 18 arc-sec, and (c) 5 by 3 sec (~90 m). Red boxes, boundaries of the telescoping grids for the forecast model.

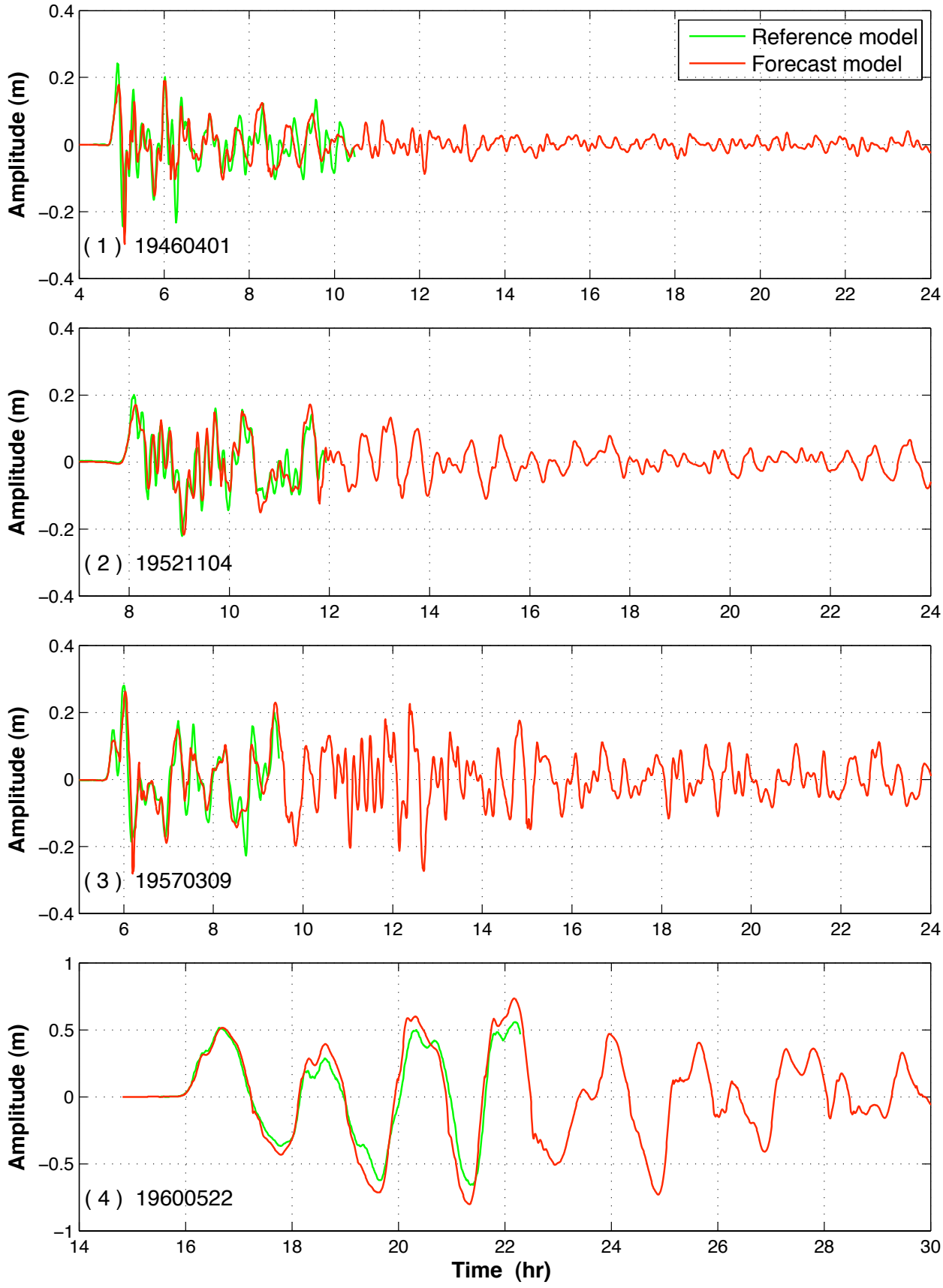
Reference model
Forecast model
Amplitude (m)
(1) 19460401
(2) 19521104
(3) 19570309
(4) 19600522
Time (hr)

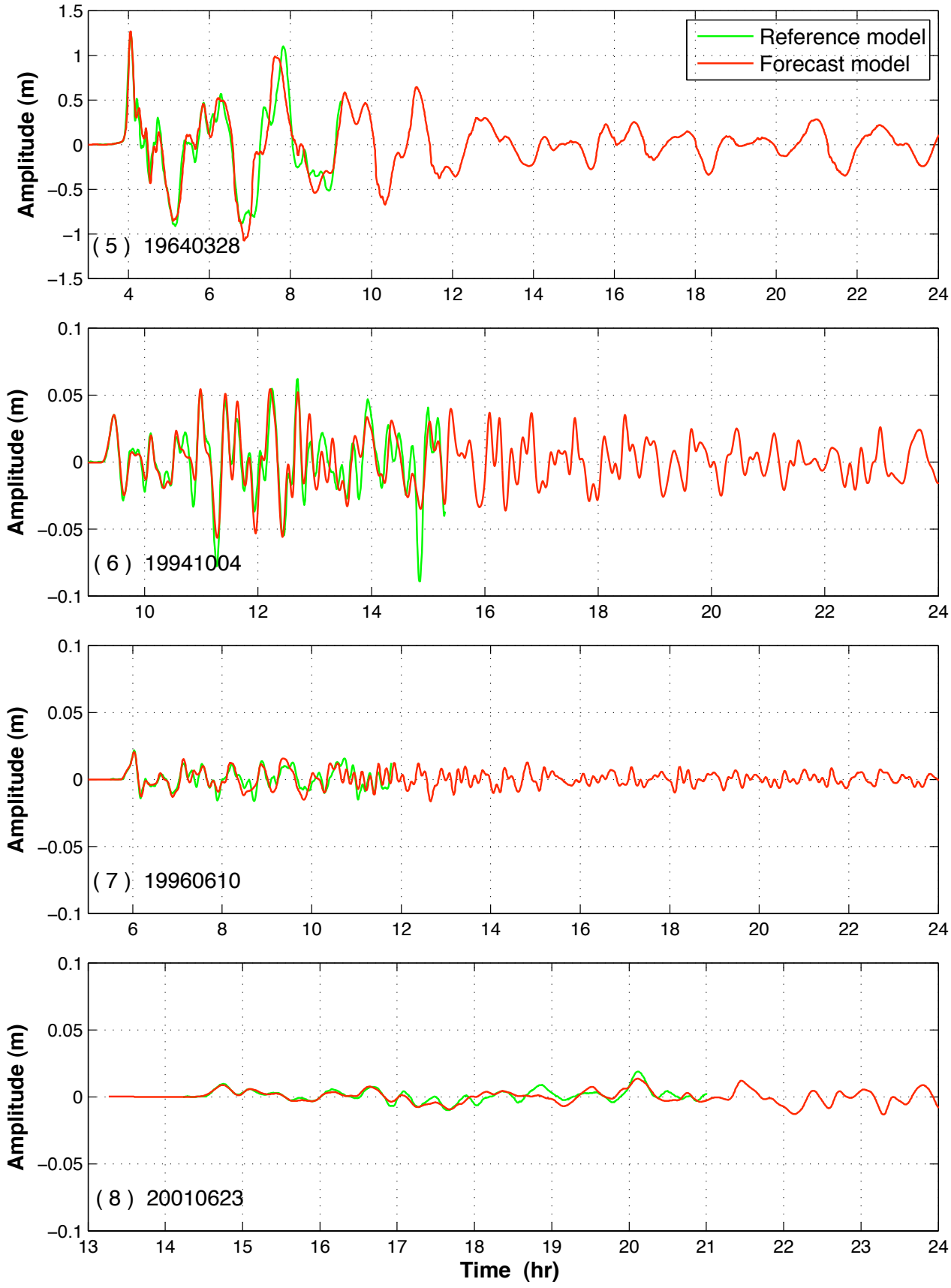
Reference model
Forecast model
Amplitude (m)
(5) 19640328
(6) 19941004
(7) 19960610
(8) 20010623
Time (hr)

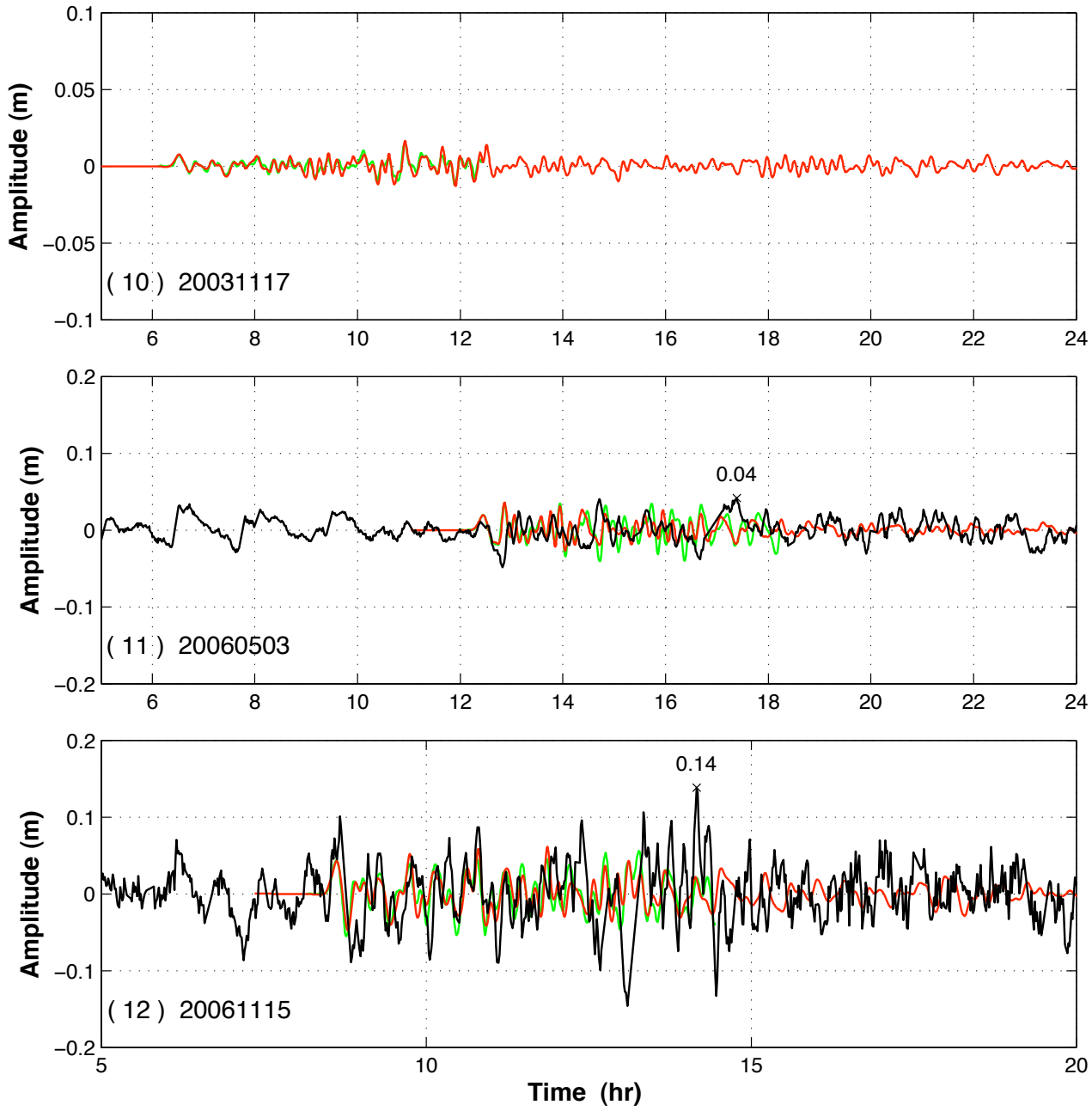
Amplitude (m)
(10) 20031117
(11) 20060503
0.04
(12) 20061115
0.14
Time (hr)

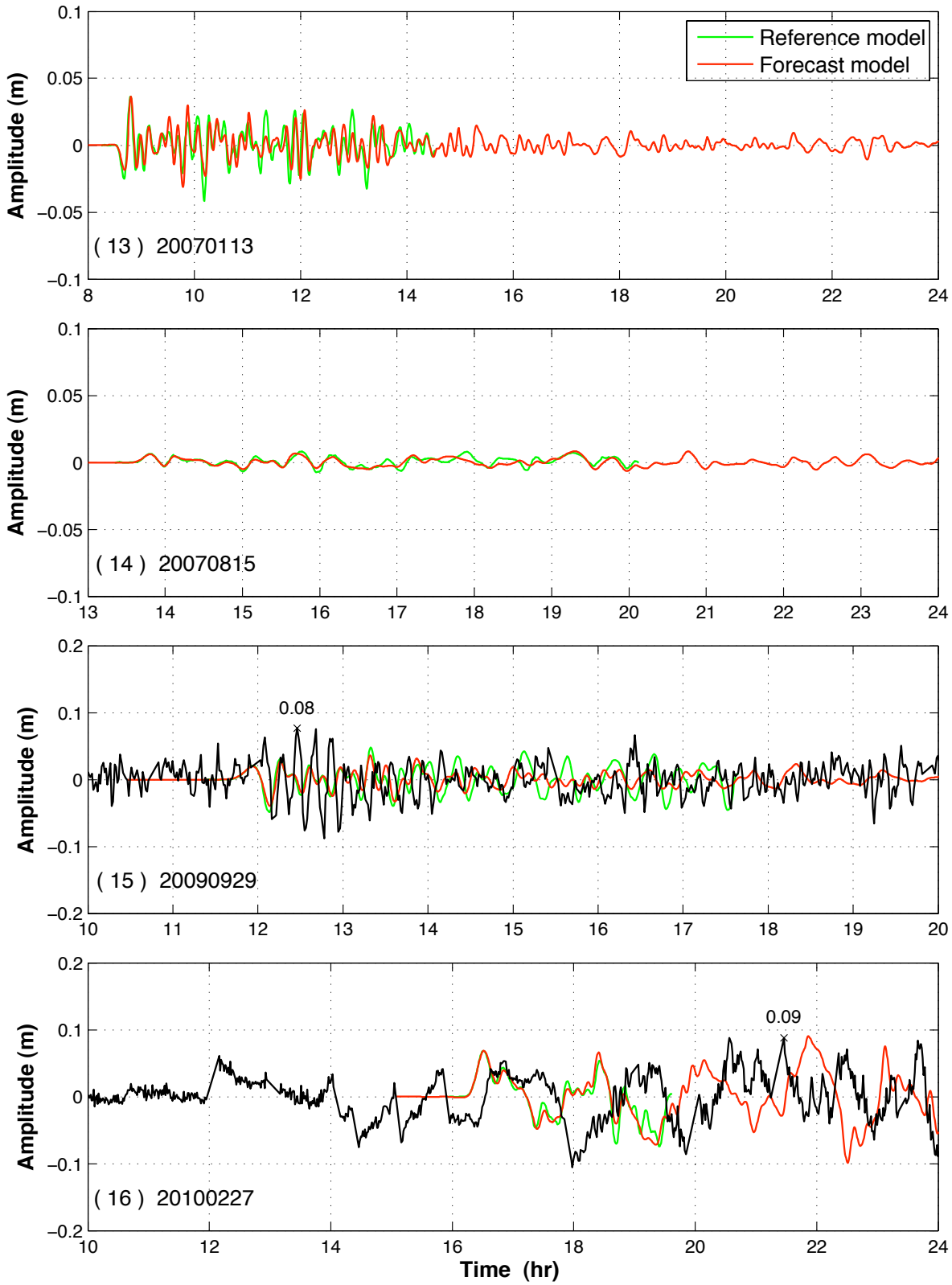

Figure 6 Observed and computed tsunami amplitude time series for sixteen past tsunamis. Black, observations; red forecast model; green, reference model.

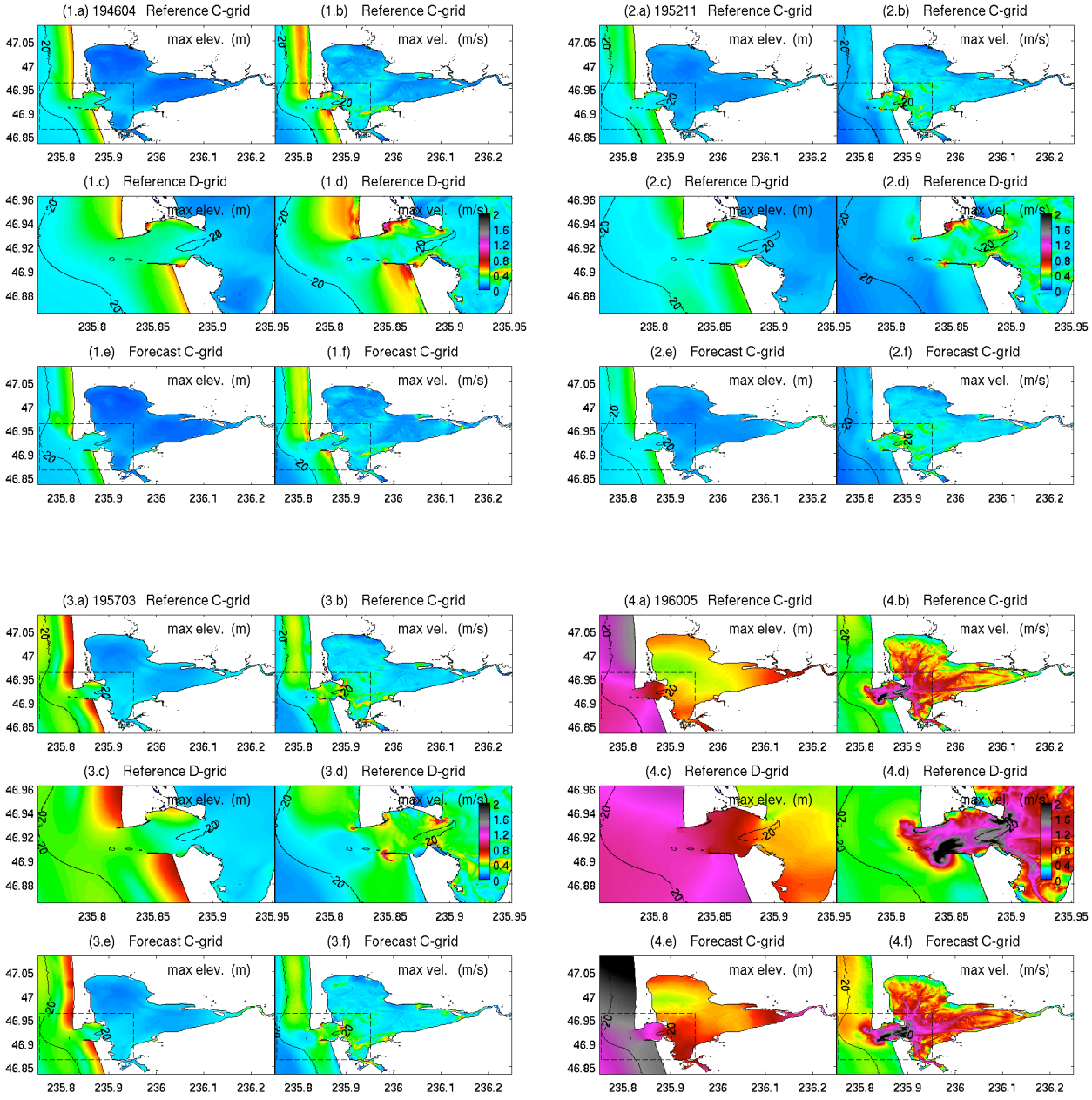
(1.a) 194604 Reference C-grid
max elev. (m)
(1.b) Reference C-grid
max vel. (m/s)
(2.a) 195211 Reference C-grid
max elev. (m)
(2.b) Reference C-grid
max vel. (m/s)
(1.c) Reference D-grid
max elev. (m)
(1.d) Reference D-grid
max vel. (m/s)
(2.c) Reference D-grid
max elev. (m)
(2.d) Reference D-grid
max vel. (m/s)
(1.e) Forecast C-grid
max elev. (m)
(1.f) Forecast C-grid
max vel. (m/s)
(2.e) Forecast C-grid
max elev. (m)
(2.f) Forecast C-grid
max vel. (m/s)
(3.a) 195703 Reference C-grid
max elev. (m)
(3.b) Reference C-grid
max vel. (m/s)
(4.a) 196005 Reference C-grid
max elev. (m)
(4.b) Reference C-grid
max vel. (m/s)
(3.c) Reference D-grid
max elev. (m)
(3.d) Reference D-grid
max vel. (m/s)
(4.c) Reference D-grid
max elev. (m)
(4.d) Reference D-grid
max vel. (m/s)
(3.e) Forecast C-grid
max elev. (m)
(3.f) Forecast C-grid
max vel. (m/s)
(4.e) Forecast C-grid
max elev. (m)
(4.f) Forecast C-grid
max vel. (m/s)

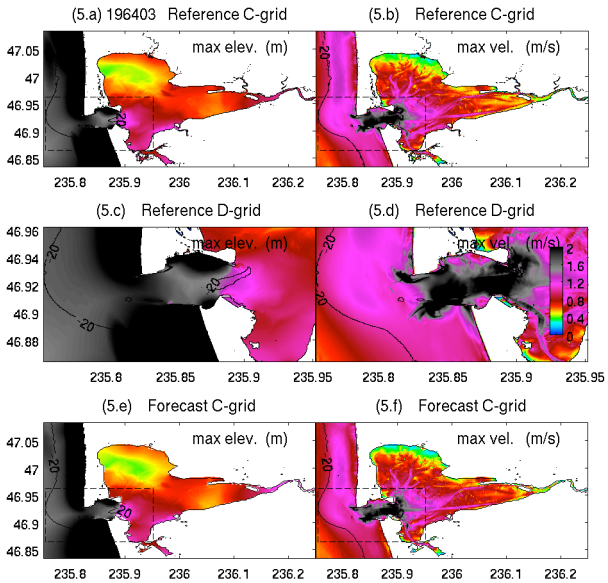
(5.a) 196403 Reference C-grid
max elev. (m)
(5.b) Reference C-grid
max vel. (m/s)
(5.c) Reference D-grid
max elev. (m)
(5.d) Reference D-grid
max vel. (m/s)
(5.e) Forecast C-grid
max elev. (m)
(5.f) Forecast C-grid
max vel. (m/s)

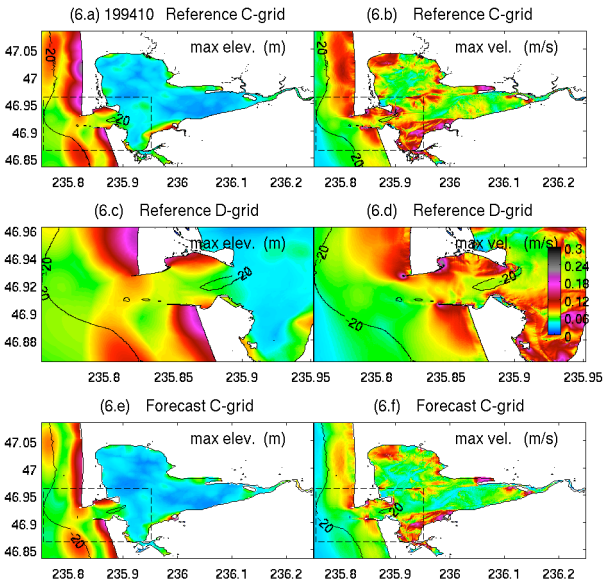
(6.a) 199410 Reference C-grid
max elev. (m)
(6.b) Reference C-grid
max vel. (m/s)
(6.c) Reference D-grid
max elev. (m)
(6.d) Reference D-grid
max vel. (m/s)
(6.e) Forecast C-grid
max elev. (m)
(6.f) Forecast C-grid
max vel. (m/s)

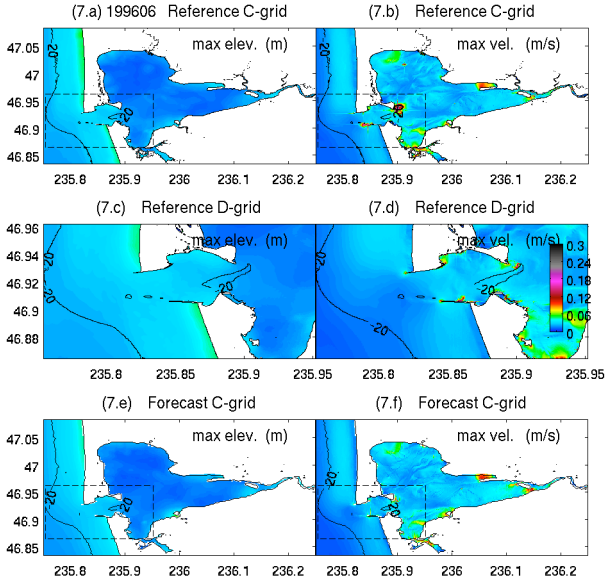
(7.a) 199606 Reference C-grid
max elev. (m)
(7.b) Reference C-grid
max vel. (m/s)
(7.c) Reference D-grid
max elev. (m)
(7.d) Reference D-grid
max vel. (m/s)
(7.e) Forecast C-grid
max elev. (m)
(7.f) Forecast C-grid
max vel. (m/s)

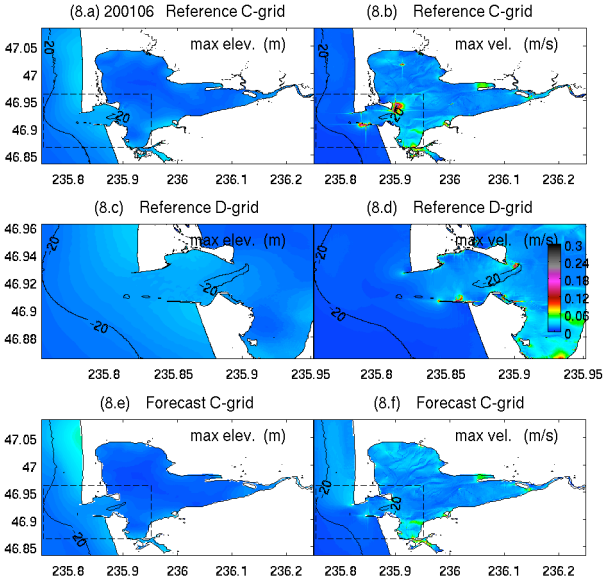
(8.a) 200106 Reference C-grid
max elev. (m)
(8.b) Reference C-grid
max vel. (m/s)
(8.c) Reference D-grid
max elev. (m)
(8.d) Reference D-grid
max vel. (m/s)
(8.e) Forecast C-grid
max elev. (m)
(8.f) Forecast C-grid
max vel. (m/s)

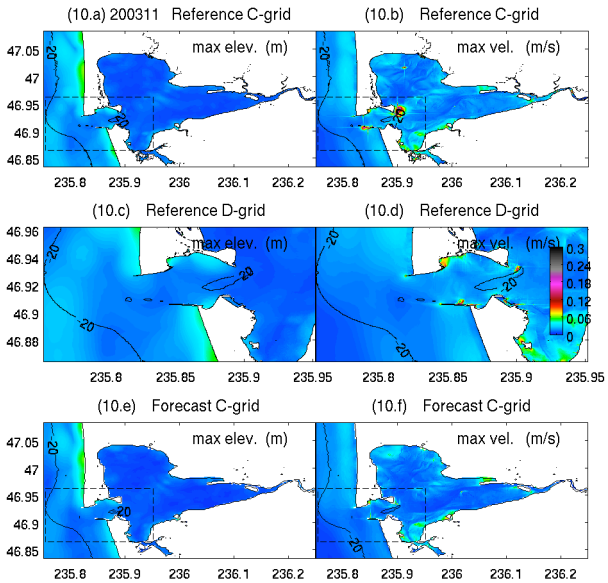
(10.a) 200311 Reference C-grid
max elev. (m)
(10.b) Reference C-grid
max vel. (m/s)
(10.c) Reference D-grid
max elev. (m)
(10.d) Reference D-grid
max vel. (m/s)
(10.e) Forecast C-grid
max elev. (m)
(10.f) Forecast C-grid
max vel. (m/s)

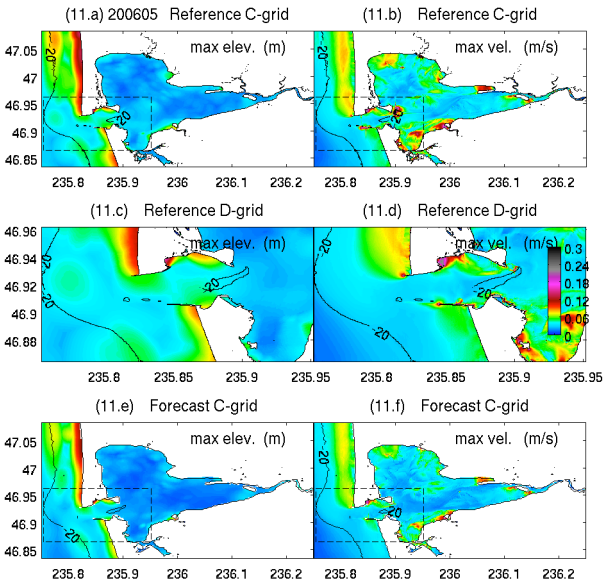
(11.a) 200605 Reference C-grid
max elev. (m)
(11.b) Reference C-grid
max vel. (m/s)
(11.c) Reference D-grid
max elev. (m)
(11.d) Reference D-grid
max vel. (m/s)
(11.e) Forecast C-grid
max elev. (m)
(11.f) Forecast C-grid
max vel. (m/s)

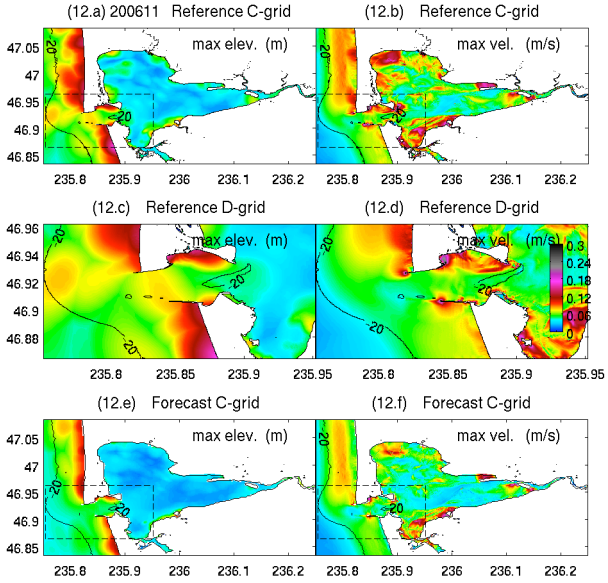
(12.a) 200611 Reference C-grid
max elev. (m)
(12.b) Reference C-grid
max vel. (m/s)
(12.c) Reference D-grid
max elev. (m)
(12.d) Reference D-grid
max vel. (m/s)
(12.e) Forecast C-grid
max elev. (m)
(12.f) Forecast C-grid
max vel. (m/s)

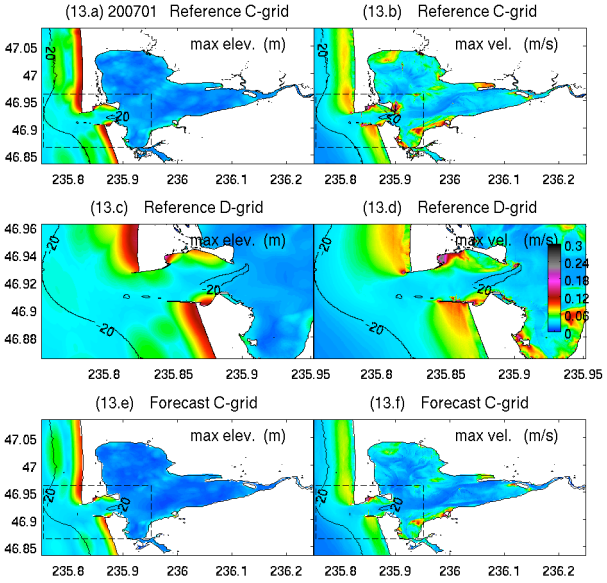
(13.a) 200701 Reference C-grid
max elev. (m)
(13.b) Reference C-grid
max vel. (m/s)
(13.c) Reference D-grid
max elev. (m)
(13.d) Reference D-grid
max vel. (m/s)
(13.e) Forecast C-grid
max elev. (m)
(13.f) Forecast C-grid
max vel. (m/s)

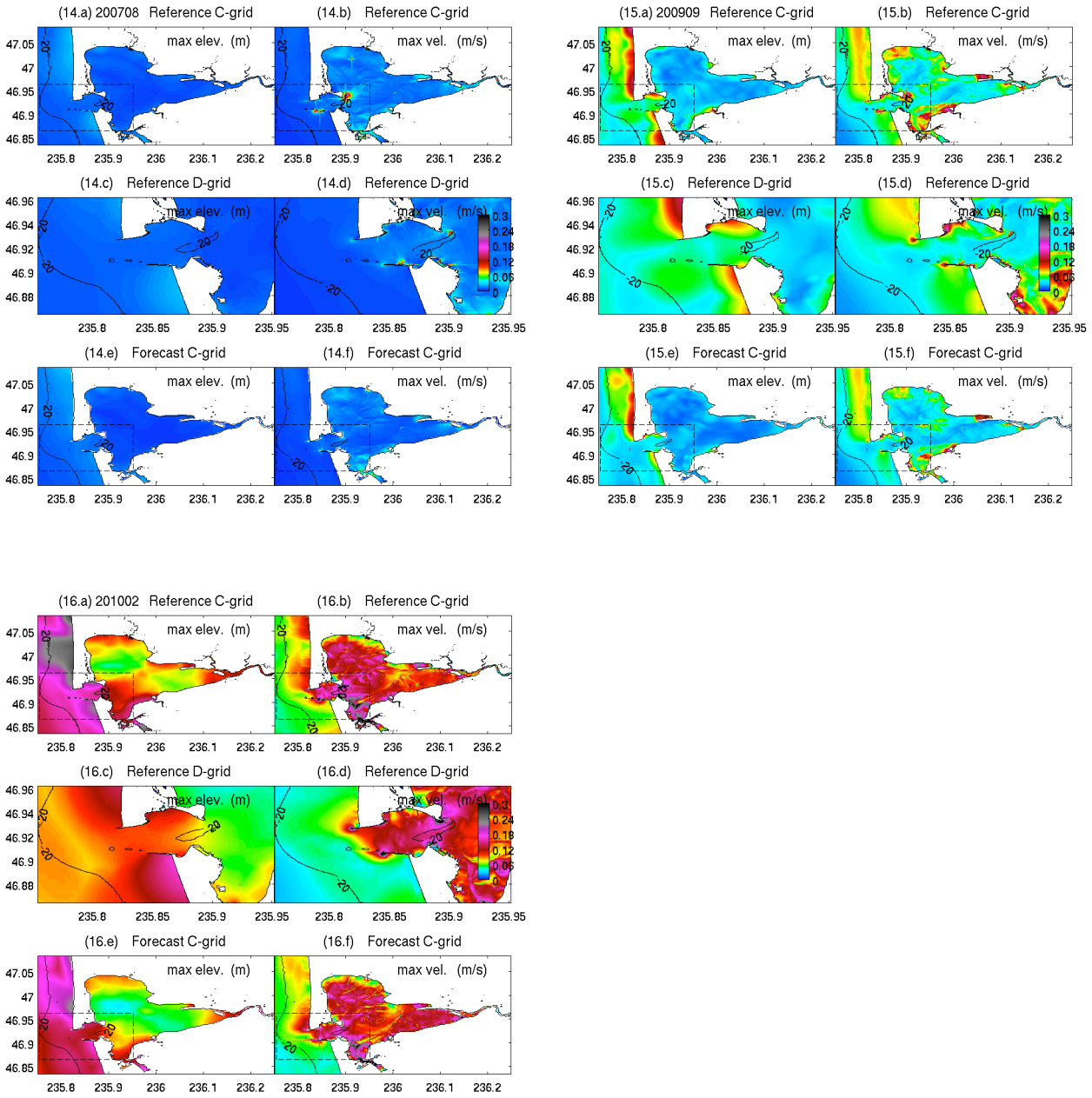

Figure 7 Computed maximum amplitude and current in the (a and b) C-grid and (c and d) D-grid of the reference model, and (e and f) C-grid of the forecast model for the sixteen past tsunamis.

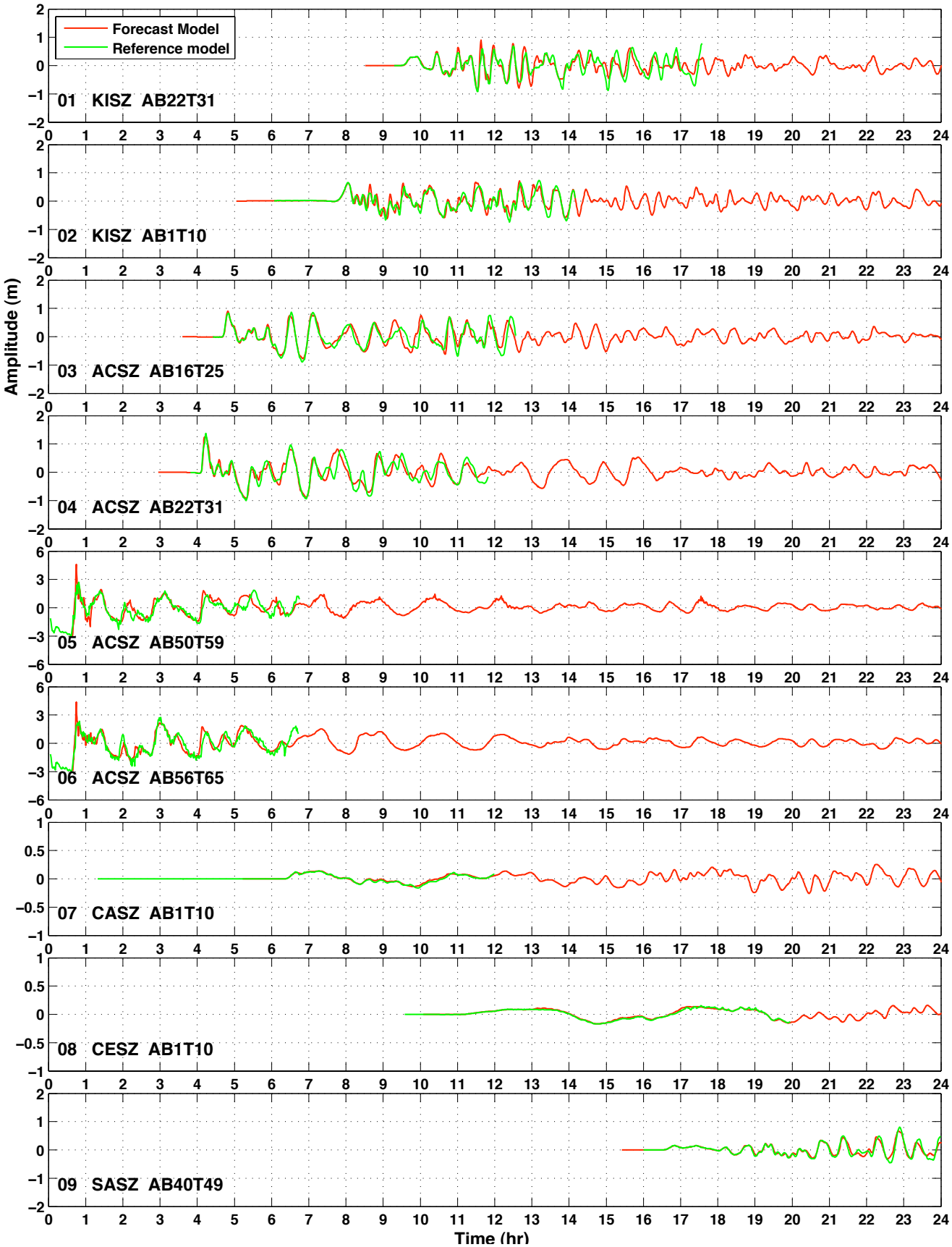
Forecast Model
Reference model
01 KISZ AB22T31
02 KISZ AB1T10
03 ACSZ AB16T25
04 ACSZ AB22T31
05 ACSZ AB50T59
06 ACSZ AB56T65
07 CASZ AB1T10
08 CESZ AB1T10
09 SASZ AB40T49
Amplitude (m)
Time (hr)

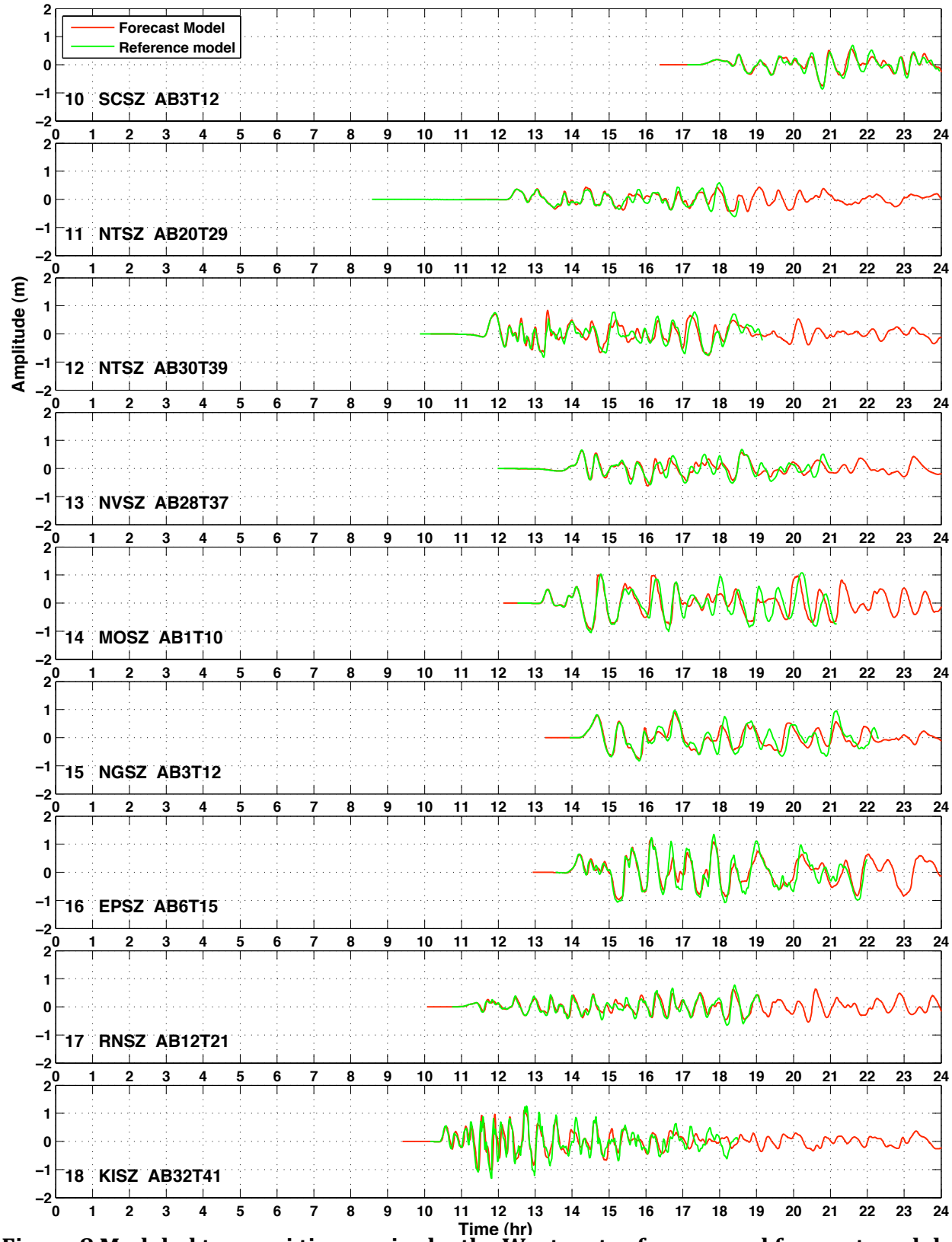

Figure 8 Modeled tsunami time series by the Westport reference and forecast models for simulated magnitude 9.3 tsunamis. Locations of the tsunamis can be found in Figure 1.

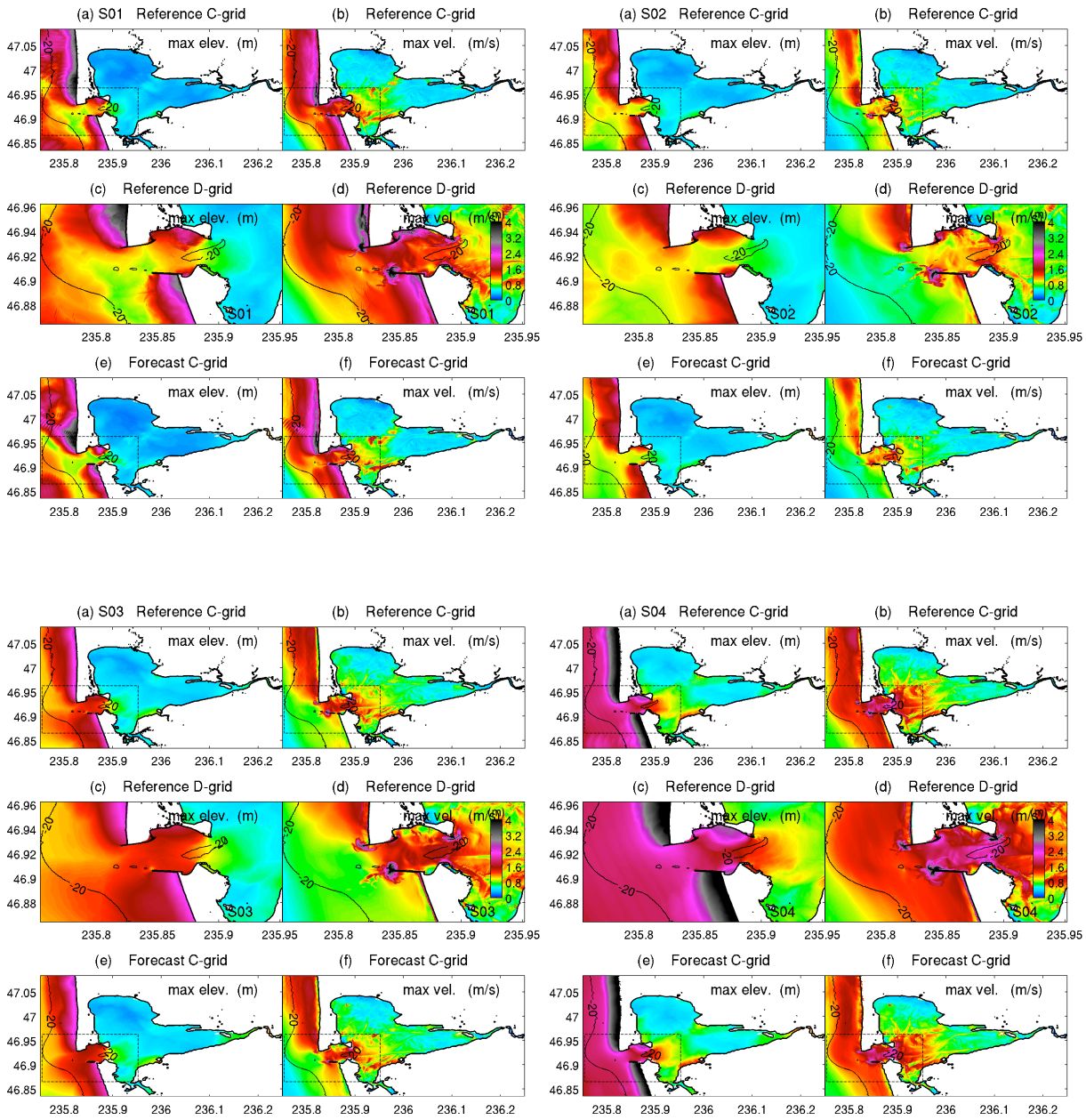
(a) S01 Reference C-grid
(b) Reference C-grid
(c) Reference D-grid
(d) Reference D-grid
(e) Forecast C-grid
(f) Forecast C-grid
(a) S02 Reference C-grid
(b) Reference C-grid
(c) Reference D-grid
(d) Reference D-grid
(e) Forecast C-grid
(f) Forecast C-grid
max elev. (m)
max vel. (m/s)
S01
S02
S03
S04

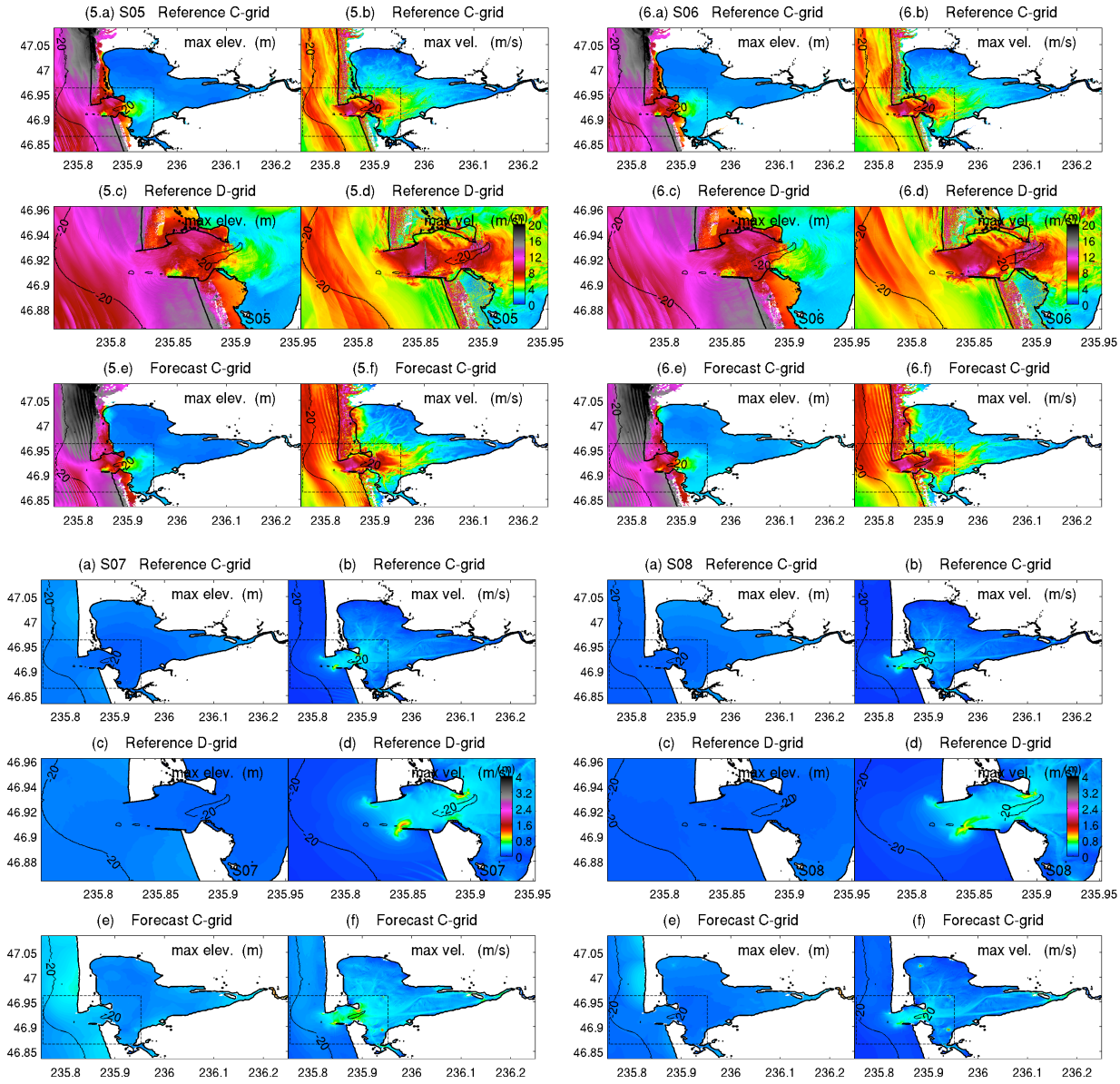
(5.a) S05 Reference C-grid
(5.b) Reference C-grid
(6.a) S06 Reference C-grid
(6.b) Reference C-grid
(5.c) Reference D-grid
(5.d) Reference D-grid
(6.c) Reference D-grid
(6.d) Reference D-grid
(5.e) Forecast C-grid
(5.f) Forecast C-grid
(6.e) Forecast C-grid
(6.f) Forecast C-grid
(a) S07 Reference C-grid
(b) Reference C-grid
(a) S08 Reference C-grid
(b) Reference C-grid
(c) Reference D-grid
(d) Reference D-grid
(c) Reference D-grid
(d) Reference D-grid
(e) Forecast C-grid
(f) Forecast C-grid
(e) Forecast C-grid
(f) Forecast C-grid
max elev. (m)
max vel. (m/s)
S05
S06
S07
S08

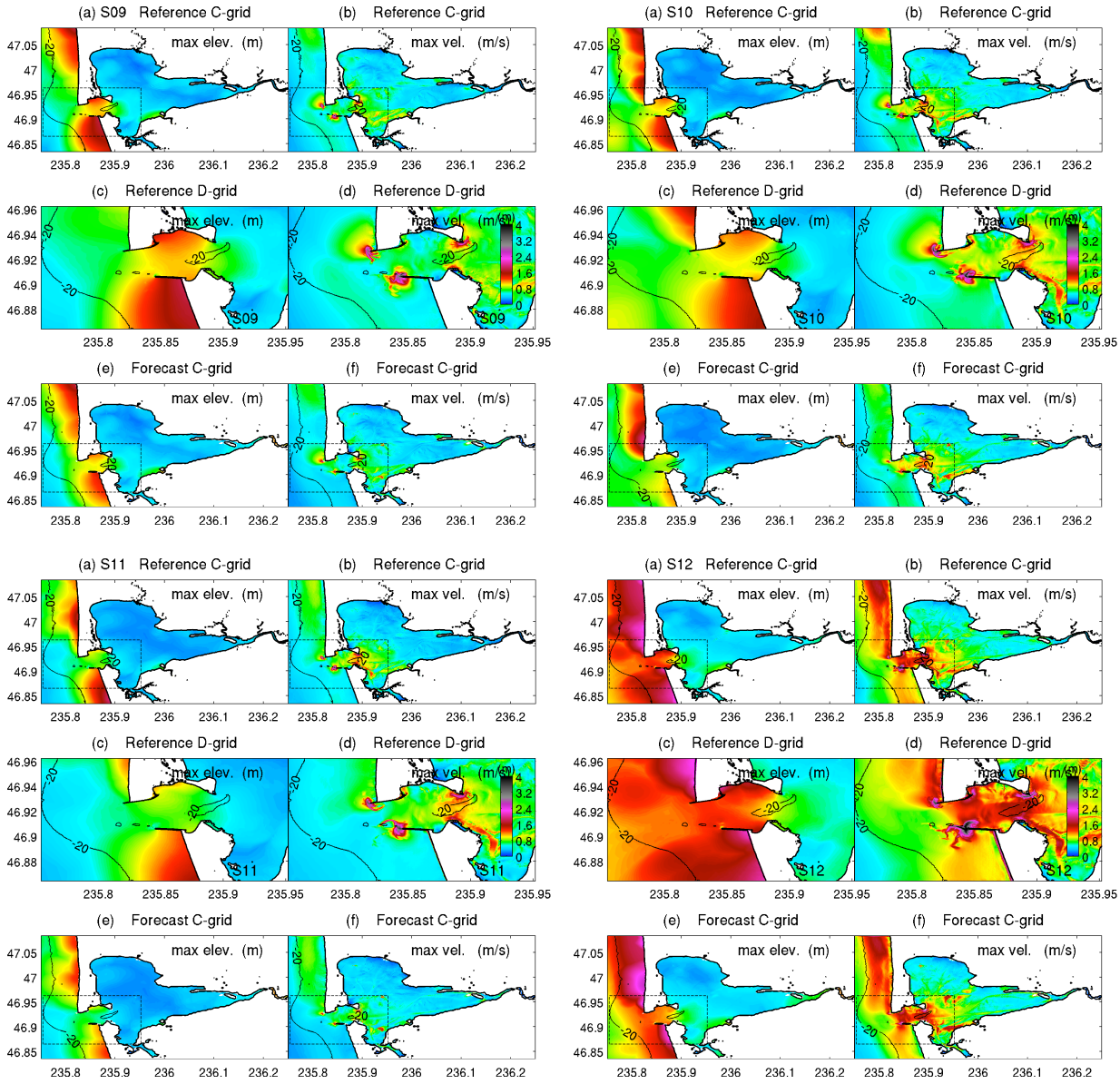
(a) S09 Reference C-grid
(b) Reference C-grid
(c) Reference D-grid
(d) Reference D-grid
(e) Forecast C-grid
(f) Forecast C-grid
(a) S10 Reference C-grid
(b) Reference C-grid
(c) Reference D-grid
(d) Reference D-grid
(e) Forecast C-grid
(f) Forecast C-grid
(a) S11 Reference C-grid
(b) Reference C-grid
(c) Reference D-grid
(d) Reference D-grid
(e) Forecast C-grid
(f) Forecast C-grid
(a) S12 Reference C-grid
(b) Reference C-grid
(c) Reference D-grid
(d) Reference D-grid
(e) Forecast C-grid
(f) Forecast C-grid
max elev. (m)
max vel. (m/s)
S09
S10
S11
S12

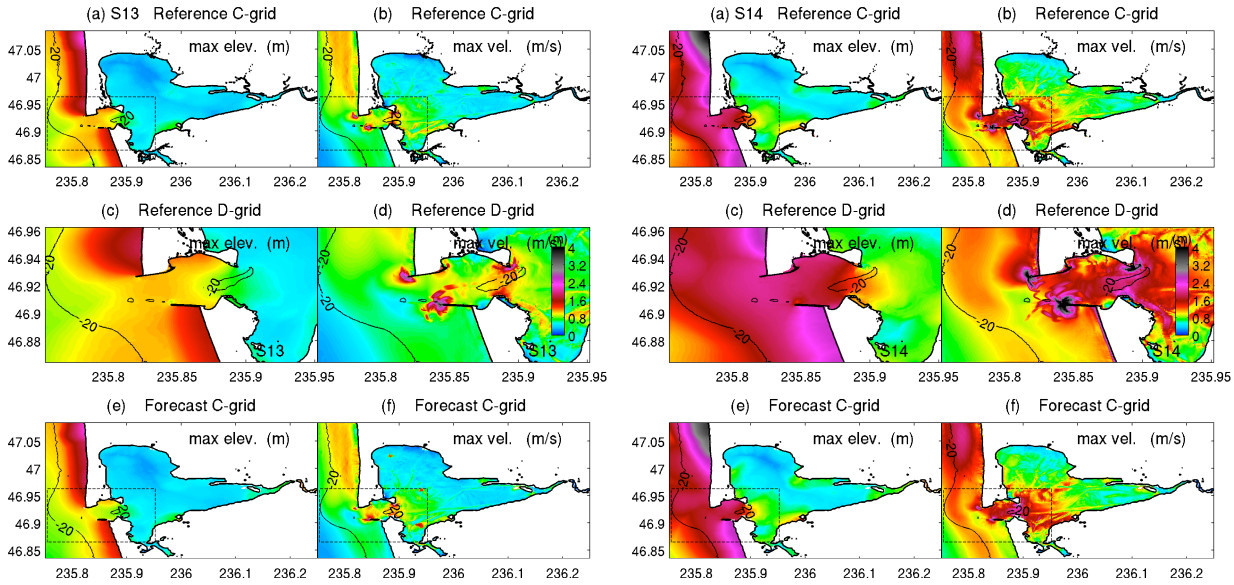
(a) S13 Reference C-grid
(b) Reference C-grid
(c) Reference D-grid
(d) Reference D-grid
(e) Forecast C-grid
(f) Forecast C-grid
max elev. (m)
max vel. (m/s)
S13
(a) S14 Reference C-grid
(b) Reference C-grid
(c) Reference D-grid
(d) Reference D-grid
(e) Forecast C-grid
(f) Forecast C-grid
max elev. (m)
max vel. (m/s)
S14

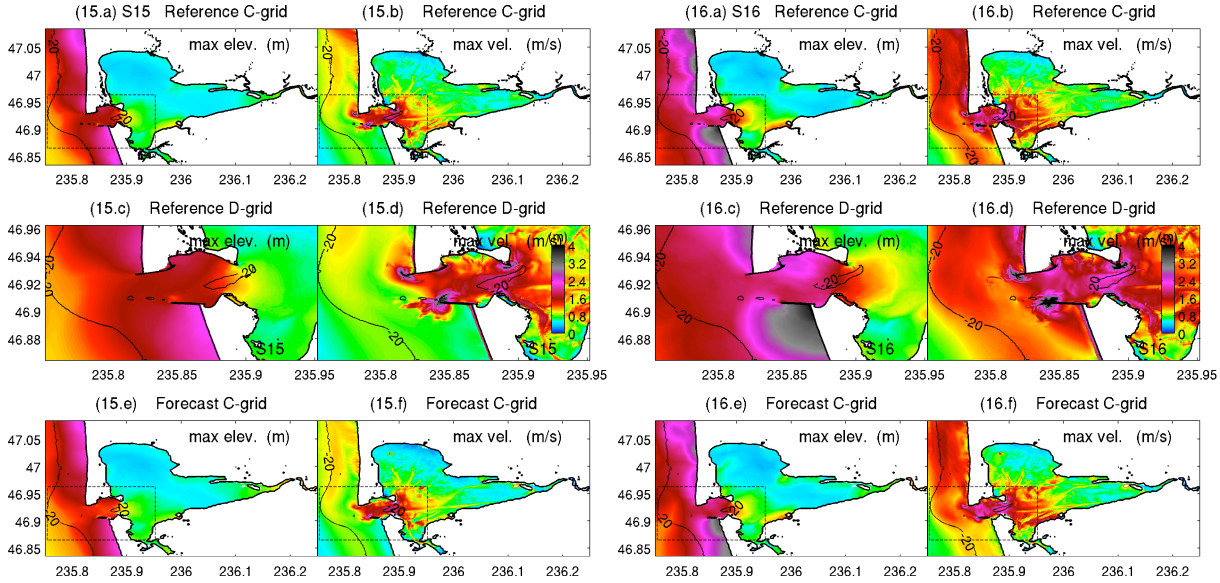
(15.a) S15 Reference C-grid
(15.b) Reference C-grid
(15.c) Reference D-grid
(15.d) Reference D-grid
(15.e) Forecast C-grid
(15.f) Forecast C-grid
max elev. (m)
max vel. (m/s)
S15
(16.a) S16 Reference C-grid
(16.b) Reference C-grid
(16.c) Reference D-grid
(16.d) Reference D-grid
(16.e) Forecast C-grid
(16.f) Forecast C-grid
max elev. (m)
max vel. (m/s)
S16

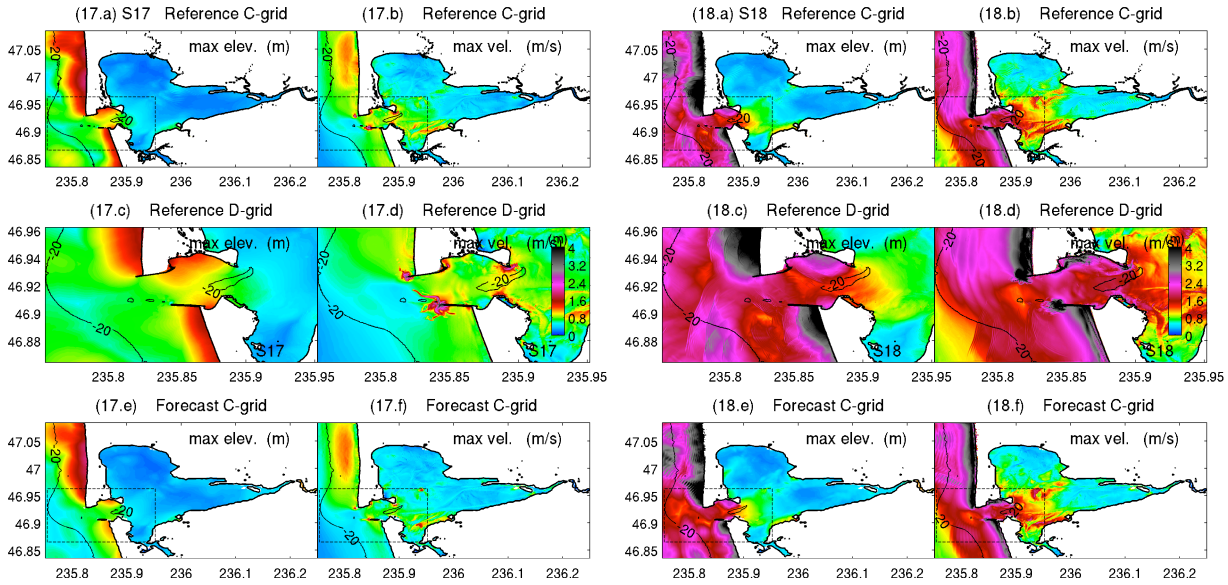

Figure 9 Computed maximum amplitude and current in the (a and b) C-grid and (a and d) D-grid of the reference model, and (e and f) C-grid of the forecast model for the simulated magnitude 9.3 tsunamis.

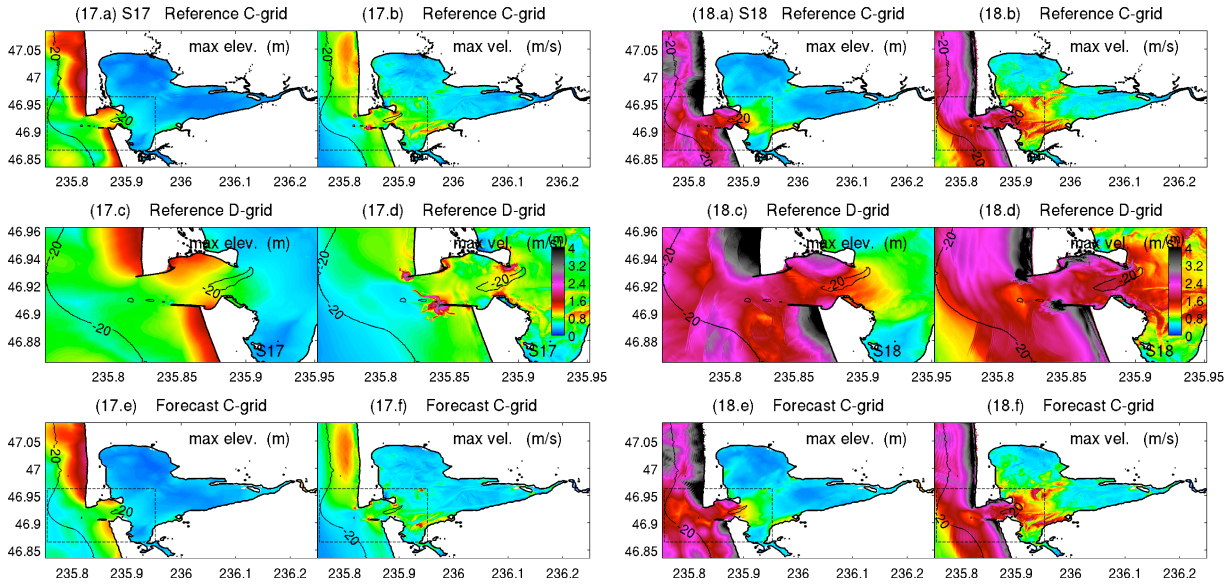

Figure 9 Computed maximum amplitude and current in the (a and b) C-grid and (a and d) D-grid of the reference model, and (e and f) C-grid of the forecast model for the simulated magnitude 9.3 tsunamis.